Orthogonal Biophysical Decision Framework

Integrated Orthogonal Biophysical Characterization for Drug-Discovery Decision Making

Integrating complementary biophysical techniques into a unified decision framework that systematically reduces experimental uncertainty and enables confident drug-discovery decisions.

Target..... Target 1
Project..... Orthogonal Biophysical Decision Framework
Client.....Confidential
Project No.....VB-2026-001
ReportVersion..... 1.0
Scientific Lead..... Todd W. Pascarella
Date..... June 2026

CONFIDENTIALITY

This report contains confidential and proprietary information generated by Valenthos Biophysics LLC on behalf of the client. The contents of this document are intended solely for the client and authorized representatives. Redistribution or disclosure of this material without written permission from Valenthos Biophysics LLC is prohibited.

Todd W. Pascarella
Director of Biophyisics Development, Biophysics
Phone: +1 (215) 490-5841
Pascarella.Todd@Valenthosbio.com

EXECUTIVE SUMMARY

Scientific Question

Can Target 1 be confidently advanced as a biophysically tractable drug-discovery target, and do the evaluated ligands specifically engage the target while preserving its structural integrity? Furthermore, if binding is confirmed, which ligand should be prioritized for medicinal chemistry optimization, and what aspects of the molecular interaction should guide future structure–activity relationship (SAR) efforts?

Orthogonal Biophysical Strategy

Unlike conventional assay reports that present individual experimental outputs independently, the Orthogonal Biophysical Decision Framework integrates complementary measurements into a unified mechanistic model that systematically reduces experimental uncertainty and provides actionable guidance for medicinal chemistry and project decision-making.

Rather than relying on a single experimental technique, an integrated orthogonal biophysical workflow was employed in which each method addressed a distinct source of experimental uncertainty.

Scientific Question	Orthogonal Technique(s)
Is the protein intact and suitable for study?	SDS-PAGE
Is the protein properly folded?	Circular Dichroism (CD)
Does the protein remain monodisperse in solution?	Analytical Size-Exclusion Chromatography (aSEC)
Is the protein sufficiently stable under assay conditions?	Differential Scanning Fluorimetry (DSF)
Do the ligands bind in solution?	TRIC
Do fluorescent ligands specifically engage the target?	Fluorescence Polarization (FP)
What are the binding affinity, kinetics, residence time, and target occupancy?	Surface Plasmon Resonance (SPR)
What are the thermodynamic driving forces of binding?	Isothermal Titration Calorimetry (ITC)

The convergence of these complementary methodologies substantially reduces experimental uncertainty by independently validating protein quality, molecular recognition, structural integrity, binding kinetics, equilibrium affinity, target occupancy, and thermodynamic mechanism.

Executive Findings

Target 1

Orthogonal quality-control experiments demonstrated that Target 1 is a properly folded, predominantly β-sheet glycoprotein that remains monodisperse, structurally intact, and compatible with quantitative biophysical characterization. Although increasing DMSO concentrations produced modest thermal destabilization, the protein maintained a cooperative unfolding transition under all assay conditions employed.

Ligand_1

Direct target engagement was independently confirmed by SPR, ITC, DSF, and TRIC. Across all orthogonal techniques, Ligand_1 consistently exhibited the highest affinity for Target 1. SPR demonstrated slower dissociation, approximately 30% greater target occupancy, and a substantially longer residence time than Ligand_2, indicating formation of the most kinetically stable protein–ligand complex. Despite strong binding, no detectable changes in secondary structure, oligomeric state, or global solution behavior were observed, while DSF demonstrated reproducible stabilization of the native protein by approximately +2.5°C.

Ligand_2

Ligand_2 likewise demonstrated direct and specific interaction with Target 1 across SPR, ITC, DSF, and TRIC. Although the compound produced thermal stabilization comparable to Ligand_1 and preserved the structural integrity of the protein, SPR revealed lower target occupancy, faster dissociation, and a shorter residence time, identifying Ligand_2 as a slightly weaker yet fully validated binder.

Fluorescent Tracers

Ligand_1-Alexa643 and Ligand_2-Alexa643 retained specific Target 1 recognition following fluorescent labeling. Fluorescence polarization experiments demonstrated reproducible concentration-dependent binding with no measurable interaction with the lysozyme negative control, validating both probes for future target-engagement, competition, and assay-development studies.

Scientific Decision

The orthogonal dataset converges on a single mechanistic model.

Target 1 is a robust, assay-compatible protein suitable for ligand-discovery and lead-optimization programs. Both Ligand_1 and Ligand_2 specifically recognize the same or highly overlapping native conformational state without inducing detectable global structural rearrangements. Instead, ligand binding stabilizes the existing folded ensemble while preserving secondary structure, oligomeric state, and solution behavior.

The principal distinction between the compounds resides not in how they bind, but in how long they remain bound. SPR demonstrates that Ligand_1 forms a more kinetically stable complex characterized by slower dissociation, longer residence time, and greater target occupancy. ITC further indicates that both interactions are predominantly enthalpy-driven, suggesting that optimization of local intermolecular contacts rather than wholesale scaffold redesign is the most promising direction for future medicinal chemistry.

Recommended Next Steps

Advance **Ligand_1** as the primary lead compound for continued SAR optimization and functional characterization.

Maintain **Ligand_2** as an important comparator for defining the structural determinants governing affinity, residence time, and productive target engagement.

Retain **Ligand_1-Alexa643** and **Ligand_2-Alexa643** as validated fluorescent tracers for future target-engagement, competition, and screening assays.

Future chemistry efforts should prioritize improving aqueous solubility while preserving the current binding scaffold and strengthening intermolecular interactions that further reduce the dissociation rate and extend target residence time.

EXECUTIVE BIOPHYSICAL ASSESSMENT DASHBOARD

To facilitate decision-making, the results obtained from all orthogonal biophysical techniques were integrated into a single comparative assessment. Each ligand was evaluated based on evidence of direct target engagement, measured binding affinity, thermodynamic signature, effects on protein stability, structural integrity, solution behavior, and aggregation propensity. The objective of this analysis was not only to confirm binding, but also to determine whether ligand association produced favorable biophysical properties consistent with further development.

Collectively, the data demonstrate that Ligand_1 and Ligand_2 engage Target 1 through specific interactions that were independently confirmed by DSF, TRIC, and ITC. Both compounds increased the thermal stability of Target 1 without inducing detectable changes in secondary structure, oligomerization state, or solution homogeneity. Thermodynamic analysis further indicates that binding is driven by favorable enthalpic and entropic contributions, supporting the formation of energetically favorable protein–ligand complexes.

The fluorescent derivatives Ligand_1-Alexa643 and Ligand_2-Alexa643 similarly demonstrated specific target engagement by fluorescence polarization; however, a complete orthogonal characterization was not performed for these compounds.

The integrated assessment summarized in Table 1 consolidates all experimental observations and provides a data-driven framework for ligand prioritization and future structure–activity relationship (SAR) efforts.

Table 1. Summary of Ligand Effects on Target 1 Binding, Stability, Structure, and Solution Behavior.

Ligand	Binding	$K_{D,app}$ (DSF)	$K_{D,app}$ (TRIC)	$K_{D,app}$ (FP)	K_D (SPR)	K_D (ITC)	Binding driven by:	Stability	Structure	Oligomerization	Aggregation	Recommendation
Ligand_1	✓	**4** µM	4 µM	ND	3.5 µM	3.4 µM	Enthalpy-driven with an entropic penalty	↑ +2.5 ^{0}C	No change	No	**Ligand yes**	Advance
Ligand_2	✓	**8** µM	7 µM	ND	5 µM	6.5 µM	Enthalpy-driven with an entropic penalty	↑ +2.5 ^{0}C	No change	No	**Ligand yes**	Advance
Ligand_1-Alexa643	✓	ND	ND	3 µM	ND	ND	ND	ND	ND	ND	**Ligand yes**	Validated fluorescent tracer
Ligand_2-Alexa643	✓	ND	ND	7 µM	ND	ND	ND	ND	ND	ND	**Ligand yes**	Validated fluorescent tracer

INTEGRATED BIOPHYSICAL CHARACTERIZATION SUMMARY (DETAILED RESULTS)

Table 2. Integrated Assessment of Target 1 and Associated Ligands.

Ligand	Target 1 Apo	Ligand_1	Ligand_2	Ligand_1-Alexa643	Ligand_2-Alexa643
DMSO EFFECT BY DSF	Small destabilization (-2 ^{0}C) at 5% DMSO.	N/A	N/A	N/A	N/A
DSF ΔT_m (°C)	T_m at 48 ^{0}C	+2.5	+2.5	ND	ND
DSF $K_{D,app}$ (µM)	N/A	4.0 µM	8.0 µM	ND	ND
DSF thermogram Interpretation	Target 1 APO shows a defined thermal transition with an apparent T_m of 48.0°C.	Ligand_1 and Ligand_2, shifts T_m to 50.5°C, corresponding to a +2.5°C stabilization for both ligands.		ND	ND
TRIC $K_{D,app}$ (µM)	N/A	4.0 µM	7.0 µM	ND	ND
FP $K_{D,app}$ (µM)	N/A	ND	ND	3.0 µM	7.0 µM
ITC K_D (µM)	N/A	3.4 µM	6.5 µM	ND	ND
Stoich. (N)	N/A	0.91	0.99	ND	ND
ΔH (kcal/mol)	N/A	-25.4	-22.5 kcal/mol	ND	ND
-TΔS (kcal/mol)	N/A	+17.9	+15.4	ND	ND
ΔG (kcal/mol)	N/A	-7.5	-7.1	ND	ND
SDS-PAGE	Target 1 migrates around 40 kDa due to glycosylation.	Comparable migration profile to Apo Target 1.	Comparable migration profile to Apo Target 1.	ND	ND
CD Change	Protein mainly β-sheet structure.	Minor stabilization.	No change.	ND	ND
aSEC R_s (nm)	2. 43	2.40	2.41	ND	ND
f/f_0	1.34	1.33	1,33	ND	ND
Oligomerization	No	ND	ND	ND	ND
Aggregation	No	Ligand Aggregation.	Ligand Aggregation.	Ligand Aggregation.	Ligand Aggregation.
k_{on} (SPR) ($mol^{-1}s^{-1}$)	N/A	1.69E+04	1.95E+04	1.07E+04	1.69E+04
k_{off} (SPR) (s^{-1})	N/A	5.96E-02	9.89E-02	7.60E-02	1.22E-01
$K_{D,app}$ µM (SPR kinetics)	N/A	3.5 µM	5.0 µM	7.0 µM	7.2 µM
Retention Time (s)	N/A	17 s	10 s	13 s	8 s
K_D (steady-state SPR)	N/A	1.6 µM	7.8 µM	6.4 µM	8.5 µM
$K_{D,app}$ (MST)	N/A	ND	ND	7.1 µM	6.3 µM
Overall Assessment	**Validated and Assay-Compatible Protein Preparation**	**Validated Binder**	**Validated Binder**	**Validated Tracer Binder**	**Validated Tracer Binder**

N/A = Not Applicable; ND = Not Determined. *Ligands exhibited a high propensity for aggregation at 500 µM in 5% DMSO about 33% of aggregation. Aggregation was further exacerbated in the absence of 0.05% Tween-20 about 70% of aggregation.*

DECISION RATIONALE

The integrated orthogonal biophysical assessment demonstrates that Ligand_1 and Ligand _2 are both validated Target 1 binders supported by multiple independent lines of experimental evidence. Protein integrity (SDS-PAGE), secondary structure (CD), solution behavior (aSEC), thermal stability (DSF), solution-phase target engagement (TRIC), fluorescence-based binding (FP), real-time binding kinetics (SPR), and thermodynamic characterization (ITC) all converge on the same biological conclusion, substantially reducing the likelihood of assay-specific artifacts or false-positive binding assignments.

Among the compounds evaluated, Ligand _1 consistently demonstrated superior biophysical performance. SPR revealed higher affinity, approximately 30% greater target occupancy, slower dissociation, and a longer residence time, while DSF, TRIC, FP, and ITC independently reproduced the same affinity ranking. Importantly, both ligands stabilized the native conformational state of Target 1 without inducing detectable changes in secondary structure, oligomeric state, or overall solution behavior, suggesting that they recognize the same or highly overlapping binding interface while differing primarily in the stability of the resulting protein–ligand complex.

The fluorescent derivatives Ligand _1-Alexa643 and Ligand_2-Alexa643 demonstrated specific Target 1 recognition by fluorescence polarization and are therefore considered validated fluorescent tracers suitable for future target-engagement, competition, and assay-development studies. Because complete orthogonal characterization was not performed for the labeled derivatives, they are classified as validated tracers rather than lead compounds.

Based on the integrated orthogonal dataset, Ligand_1 is recommended as the primary lead compound for continued medicinal chemistry optimization, with future SAR efforts focusing on strengthening the existing interaction network to further reduce the dissociation rate, increase target residence time, and improve aqueous solubility while preserving the current binding mechanism. Ligand_2 remains an important comparator compound for defining the structural determinants governing affinity and kinetic stability.

Note: Interpretation of Dissociation Constants Obtained from Orthogonal Biophysical Techniques

Throughout this report, dissociation constants are interpreted within the context of the physical principle measured by each experimental technique. Although all methods provide quantitative estimates of ligand affinity, they do not measure identical molecular observables and therefore differ in the extent to which the reported values represent true thermodynamic equilibrium constants.

For Differential Scanning Fluorimetry, Temperature-Related Intensity Change, and Fluorescence Polarization, affinity values are reported as apparent dissociation constants ($K_{D,app}$) because these techniques do not directly quantify the equilibrium between free and bound molecular species. Instead, they monitor secondary physical observables that change as a consequence of ligand binding.

Specifically:

- **DSF** measures ligand-induced changes in protein thermal stability (ΔT_m).
- **TRIC** measures changes in the temperature-dependent fluorescence of a labeled protein.
- **FP** measures changes in the rotational diffusion of a fluorescent ligand.

In each case, the measured signal is related to ligand binding through an analytical binding model, and the resulting affinity therefore represents the apparent affinity governing the observed assay response under the experimental conditions employed.

Surface Plasmon Resonance directly monitors formation and dissociation of the protein–ligand complex in real time through changes in refractive index at the sensor surface. Unlike DSF, TRIC, and FP, SPR directly measures molecular binding and independently determines both kinetic (k_{on} and k_{off}) and equilibrium affinity through global kinetic and steady-state analyses. Consequently, SPR provides a direct measurement of binding affinity under the experimental conditions employed. However, because SPR measurements are performed using an immobilized target and are influenced by experimental parameters such as ligand accessibility, surface activity, and mass transport, the reported affinity values should be interpreted as equilibrium binding constants specific to the SPR assay configuration rather than absolute thermodynamic constants.

In principle, Isothermal Titration Calorimetry provides the most direct determination of the thermodynamic equilibrium dissociation constant (KD) because it measures the heat released or absorbed during molecular recognition and simultaneously determines binding stoichiometry (N), enthalpy (ΔH), entropy (ΔS), and Gibbs free energy (ΔG).

However, the present study required experimental conditions that deviated from the ideal assumptions for quantitative ITC analysis. Ligand solubility limitations restricted the maximum achievable ligand concentration, while maintenance of compound solubility required 5% DMSO. Consequently, complete saturation of the binding isotherms could not be achieved under optimal concentration conditions. Although the ITC experiments clearly demonstrate direct molecular recognition and provide reliable estimates of binding stoichiometry and thermodynamic signatures, the calculated affinity values should likewise be interpreted as apparent dissociation constants ($K_{D,app}$) that reflect the experimental conditions under which the measurements were performed.

Importantly, despite relying on fundamentally different physical principles, all orthogonal biophysical techniques employed in this study, including DSF, TRIC, FP, SPR, and ITC, converged on a consistent low-micromolar affinity range and reproduced the same affinity ranking, identifying Ligand_1 as the highest-affinity binder. The remarkable agreement among independent structural, fluorescence-based, kinetic, equilibrium, and thermodynamic measurements substantially increases confidence that the observed interactions represent genuine molecular recognition. Consequently, while the numerical affinity values remain method-dependent, the biological conclusions are supported by multiple complementary experimental approaches and should therefore be considered highly robust.

TABLE OF CONTENTS

GOAL

Evaluate the interaction between Target 1 and the test ligands and determine whether ligand binding induces measurable changes in protein structure, stability, oligomeric state, or solution behavior.

To achieve this objective, a panel of complementary orthogonal biophysical techniques was employed:

SDS-PAGE

Assess protein integrity following ligand exposure and ITC analysis by monitoring changes in electrophoretic mobility, degradation, fragmentation, precipitation, or the appearance of additional protein species.

Circular Dichroism

Evaluate whether ligand binding induces changes in protein secondary structure, folding state, or overall conformational integrity by comparing the far-UV CD spectra of apo and ligand-bound protein samples.

Analytical Size-Exclusion Chromatography

Determine whether ligand binding alters the hydrodynamic properties of Target 1 by monitoring changes in apparent molecular size, oligomeric state, aggregation propensity, Stokes radius (R_s), and frictional ratio (f/f_0). These analyses provide insight into ligand-induced conformational expansion, compaction, oligomerization, or aggregation of the target.

Differential Scanning Fluorimetry

Assess the impact of ligand binding on protein thermal stability through measurement of ligand-induced shifts in melting temperature (ΔT_m). Concentration-dependent thermal stabilization was additionally used to estimate apparent binding affinities ($K_{D,app}$) and identify compounds that stabilize or destabilize the target protein.

Temperature-Related Intensity Change

Confirm direct target engagement in solution by monitoring ligand-induced changes in the temperature-dependent fluorescence behavior of labeled Target 1. TRIC measurements were used to determine apparent binding affinities ($K_{D,app}$) and identify potential non-specific interactions or aggregation artifacts.

Fluorescence Polarization

Evaluate molecular recognition through changes in rotational mobility of a fluorescent ligand probe upon binding to Target 1. FP measurements were used to assess target occupancy, determine apparent binding affinities, and characterize competitive ligand displacement behavior.

Surface Plasmon Resonance (SPR)

Provide direct real-time characterization of protein–ligand interactions through label-free detection of molecular binding at the sensor surface. SPR was used to determine binding affinity (K_D), association and dissociation rate constants (k_{on} and k_{off}), complex residence time, maximum binding response (R_{max}), relative target occupancy, and binding stoichiometry while simultaneously assessing binding specificity, interaction kinetics, and conformity to a 1:1 binding mechanism.

Isothermal Titration Calorimetry

Provide direct thermodynamic characterization of ligand binding through measurement of heat changes associated with molecular recognition. ITC was used to determine binding affinity (K_D), stoichiometry (N), enthalpy (ΔH), entropy (ΔS), and Gibbs free energy (ΔG).

Orthogonal Biophysical Characterization Strategy

To evaluate ligand binding and determine whether target engagement alters the structural, thermodynamic, or solution properties of Target 1, a panel of complementary orthogonal biophysical techniques was employed. Each method interrogates a distinct physical property of the system and addresses a specific source of experimental uncertainty. Together, these measurements provide a comprehensive assessment of molecular recognition and ligand-induced changes in protein state.

Table 3 summarizes the role of each technique, the physical principle measured, the experimental readout generated, and the critical uncertainty addressed.

Table 3. Orthogonal Characterization Techniques Used to Reduce Experimental Uncertainty and Strengthen Biological Conclusions

Technique	Physical Principal	Read out	Critical Uncertainty Addressed
SDS-PAGE	Separation of proteins according to molecular weight in a denaturing polyacrylamide gel under an electric field.	Band pattern and apparent molecular weight.	Establishes whether the sample contains the expected protein at the correct molecular weight and purity. Eliminates uncertainty regarding degradation, truncation, contamination, or incorrect expression products. Neither CD, DSF, nor binding assays can determine whether an observed signal originates from the intended protein species or from contaminants.
Circular Dichroism (CD)	Differential absorption of left- and right-circularly polarized light by chiral molecular structures.	Ellipticity spectrum (far-UV and/or near-UV 190-260 nm).	Determines whether the protein is folded and possesses the expected secondary structure. Eliminates uncertainty regarding gross misfolding that may not be visible by SDS-PAGE. A pure protein can still be structurally compromised; CD provides structural validation that chromatography and binding assays cannot directly measure.
Analytical Size Exclusion Chromatography (aSEC)	Separation of molecules according to hydrodynamic size as they pass through a porous stationary phase.	Elution volume and chromatographic peak profile.	Determines whether the sample exists as a monomer, oligomer, aggregate, or heterogeneous mixture. Eliminates uncertainty regarding sample dispersity and aggregation. Neither SDS-PAGE nor CD can reliably detect soluble aggregates or mixed oligomeric populations that frequently generate misleading binding or stability data.

Differential Scanning Fluorimetry (DSF)	Monitoring changes in fluorescence during thermal unfolding of proteins.	Melting temperature (T_m) and unfolding profile.	Measures conformational stability and identifies conditions that stabilize or destabilize the protein. Eliminates uncertainty regarding whether the protein remains energetically stable under assay conditions. A correctly folded and monodisperse protein may still be marginally stable and unsuitable for downstream studies. DSF uniquely probes thermal robustness and ligand-induced stabilization.
Temperature-Related Intensity Change (TRIC)	Detection of temperature-dependent changes in intrinsic fluorophore emission caused by alterations in the local molecular environment.	TRIC signal amplitude and binding isotherm.	Provides direct evidence of molecular interaction in solution while requiring minimal sample consumption. Eliminates uncertainty regarding whether a ligand physically interacts with the target under native conditions. Unlike DSF, which infers binding indirectly through stability changes, TRIC directly measures concentration-dependent interaction and affinity.
Fluorescence Polarization (FP)	Measurement of rotational diffusion of fluorescent molecules through polarized light emission.	Polarization or anisotropy signal.	Determines binding, displacement, and molecular exchange processes involving fluorescently labeled species. Eliminates uncertainty regarding occupancy and competitive binding mechanisms. Unlike TRIC, which detects environmental changes, FP directly reports changes in molecular rotational freedom and is particularly powerful for competition studies and kinetic measurements.
Surface Plasmon Resonance (SPR)	Detection of changes in the refractive index at a metal sensor surface caused by biomolecular binding in real time.	Sensorgram, association rate constant (k_{on}), dissociation rate constant (k_{off}), equilibrium dissociation constant (K_D), maximum binding response (R_{max}), target occupancy, and residence time.	Determines whether a ligand binds directly to the target and quantifies both the affinity and kinetic mechanism of the interaction. Eliminates uncertainty regarding whether molecular recognition is specific, reversible, and kinetically consistent with the proposed binding model. Unlike DSF, which infers binding through changes in protein stability, or ITC, which measures the thermodynamics of complex formation, SPR directly resolves the rates of association and dissociation while simultaneously quantifying equilibrium affinity and target occupancy in real time.
Isothermal Titration Calorimetry (ITC)	Direct measurement of heat released or absorbed during molecular interactions at constant temperature.	Heat flow, binding isotherm, K_D, ΔH, ΔS, ΔG, and stoichiometry (N).	Provides the most complete physicochemical characterization of an interaction. Eliminates uncertainty regarding affinity, binding stoichiometry, and thermodynamic driving forces. Other techniques may indicate that binding occurs but cannot fully determine the mechanism by what interaction happens, or whether the observed signal corresponds to the expected molecular stoichiometry. ITC serves as the definitive orthogonal validation of molecular recognition.

RESULTS

PROTEIN AND LIGAND CONCENTRATION

This section summarizes the preparation, clarification, buffer exchange, concentration determination, and labeling quality-control procedures used for Target 1, Target 1-RED Dye, and the ligand samples prior to biophysical characterization. The objective was to define the soluble working concentration of each material after centrifugation, document visible precipitation or aggregation, estimate the degree of labeling for fluorescent species, and record the concentrations used in each experimental workflow.

Target 1

Target 1 was received as a lyophilized powder (1 mg) and reconstituted in 1 mL of water according to the client-provided instructions. The sample was incubated at room temperature for 30 min to allow complete dissolution, then centrifuged at 15,000 rpm for 20 min at 4 °C. The clarified supernatant was collected and dialyzed overnight against 20 mM HEPES, pH 7.4, 150 mM NaCl. Following dialysis, the Target 1 concentration was determined by UV absorbance at 280 nm (**Table 4**) using the calculated protein extinction coefficient (ε280 = 25,690 M^{-1} cm^{-1}). The final clarified protein stock concentration was 36.6 µM and was aliquoted into 100 µL working volumes.

Target 1-RED Dye

Target 1-RED Dye was generated using the NanoTemper Protein Labeling Kit RED-NHS 2nd Generation, as described in the Materials and Methods section. The labeled protein was exchanged into 20 mM HEPES, pH 7.4, 150 mM NaCl, 0.05% Tween-20 using buffer exchange columns. Following labeling and buffer exchange, the sample was centrifuged at 15,000 rpm for 20 min at 4 °C, and the clarified supernatant was collected. The concentration of labeled Target 1 was determined using UV-visible absorbance measurements with correction for dye contribution at 280 nm. The final Target 1-RED Dye concentration was 2.4 µM, with a degree of labeling of approximately 0.9 dye molecules per protein molecule. The sample was aliquoted into 50 µL working volumes.

Ligands

Ligands Ligand_1, Ligand_2, Ligand_1-Alexa643, and Ligand_2-Alexa643 were supplied by the client as 10 mM stocks in 100% DMSO. Each ligand was diluted to a nominal concentration of 500 µM in 20 mM HEPES, pH 7.4, 150 mM NaCl containing 5% DMSO with or without 0.05% Tween20. The diluted ligand preparations were centrifuged at 15,000 rpm for 20 min at 4 °C. Visible precipitation or aggregation was documented when present, and the clarified supernatants were collected for downstream experiments. Soluble ligand concentrations were determined by UV-visible absorbance using the ligand extinction coefficient at 280 nm (ε_{280} = 5,625 M^{-1} cm^{-1}). The clarified samples were aliquoted into 50 µL working volumes.

Degree of Labeling Calculation

For RED-dye-labeled samples, the degree of labeling (DOL) was calculated from UV-visible absorbance measurements using the dye absorbance at 650 nm and the corrected protein absorbance at 280 nm:

$$DOL = \frac{A_{650}/\varepsilon_{650,Dye}}{(A_{280} - CF * A_{650})/A_{280,protein}}$$

Where:

- A_{650} = absorbance of the dye at 650 nm
- $\varepsilon_{650,Dye}$ = molar extinction coefficient of the dye at 650 nm
- A_{280} measured absorbance at 280 nm
- CF = correction factor for dye absorbance at 280 nm
- $\varepsilon_{280,protein}$ = protein extinction coefficient at 280 nm (M^{-1} cm^{-1})

UV-Visible Quantification and Sample Quality Summary

Table 4. UV-Visible Spectroscopic Assessment of Sample Quality, Soluble Concentration, and Labeling Efficiency.

Sample	ε_{280nm} M^{-1} cm^{-1}	A280	A320	A653	DF	[ ] µM	DOL	Comment
Target 1	25690	0.94	0.07	N/A	1	36.6	N/A	Clarified protein; no visible aggregation after centrifugation.
Target 1-RED Dye	25690	0.08	0.44	0.032	1	2.4	0.9	Labeled protein recovered after clarification; DOL within an appropriate range for TRIC measurements.
Ligand_1	5625	0.39	0.02	N/A	4	277	N/A	Visible precipitation/aggregation observed. Soluble recovery ~55% relative to nominal 500 µM preparation for samples with 5% DMSO and 0.05% Tween20. For the buffer with 5% DMSO and without 0.05% Tween20 the Soluble recovery was less than 30-20%.
Ligand_2	5625	0.54	0.00	N/A	2	192	N/A	Visible precipitation/aggregation observed. Soluble recovery ~55% relative to nominal 500 µM preparation for samples with 5% DMSO and 0.05% Tween20. For the buffer with 5% DMSO and without 0.05% Tween20 the Soluble recovery was less than 30-20%.
Ligand_1-ALEXA643	5625	0.67	0.45	10.07	6	288	1.07	Visible precipitation/aggregation observed. Soluble recovery ~57%; labeled ligand DOL near 1:1.
Ligand_2-ALEXA643	5625	0.63	0.47	9.01	6	288	0.96	Visible precipitation/aggregation observed. Soluble recovery ~57%; labeled ligand DOL near 1:1.

Note. *A_{320} was used as a turbidity/light-scattering indicator. Concentrations correspond to the clarified supernatants after centrifugation and therefore represent soluble working concentrations rather than the nominal concentrations prepared before clarification. DOL = degree of labeling; DF = dilution factor; N/A = not applicable.*

Interpretation of Concentration and Quality-Control Measurements

The clarified Target 1 stock reached a final concentration of 36.6 µM with no visible aggregation, providing sufficient material for SDS-PAGE, CD, aSEC, DSF, FP, and ITC experiments. The Target 1-RED Dye preparation yielded a lower final protein concentration of 2.4 µM, which was nevertheless adequate for TRIC because the assay used

20 nM labeled protein. The measured DOL of approximately 0.9 indicates near-stoichiometric labeling and is appropriate for fluorescence-based binding assays.

The unlabeled ligands Ligand_1 and Ligand_2 showed substantial loss of soluble material after dilution from DMSO stock and centrifugation, yielding clarified concentrations of 277 µM and 192 µM, respectively. These values correspond to approximately 55% and 38% soluble recovery relative to the nominal 500 µM preparations. This observation is important for interpretation of ITC and other high-concentration assays because the usable ligand concentration was lower than the intended nominal concentration after clarification and the final buffer cannot have 0.05% Tween20.

The fluorescent ligands Ligand_1-Alexa643 and Ligand_2-Alexa643 also showed visible precipitation/aggregation after preparation but yielded similar clarified concentrations of 288 µM. Their DOL values were close to one dye per ligand molecule equivalent under the applied calculation framework (1.07 and 0.96, respectively), supporting comparable labeling quality between the two tracers. Therefore, differences observed in downstream fluorescence-based assays are unlikely to arise from major differences in labeling efficiency.

Experimental Input Concentrations

Table 5. Protein and Ligand Concentrations Used for Each Biophysical Experiment

Experiment	Target 1	Target 1-RED Dye	Ligand_1	Ligand_2	Ligand_1-Alexa643	Ligand_2-Alexa643
SDS-PAGE	3 µg	N/A	50 µM	50 µM	N/A	N/A
CD	3.7 µM	N/A	50 µM	50 µM	N/A	N/A
aSEC	10 µM	N/A	100 µM	100 µM	N/A	N/A
DSF DMSO effect	4 µM	N/A	N/A	N/A	N/A	N/A
DSF affinity	4 µM	N/A	Dose response starting at 40 µM	Dose response starting at 40 µM	N/A	N/A
TRIC affinity	N/A	20 nM	Dose response starting at 60 µM	Dose response starting at 60 µM	N/A	N/A
FP affinity	Dose response starting at 40 µM ligand	20 nM	N/A	N/A	10 nM	10 nM
ITC affinity	8-10 µM	N/A	90 µM	80 µM	N/A	N/A

Note. *The concentrations listed reflect the assay setup concentrations or starting concentrations for titration series. For dose-response experiments, serial dilution was performed from the indicated starting ligand or protein concentration.*

Overall, the sample-quality data establishes that Target 1 was obtained as a clarified, soluble protein stock suitable for orthogonal biophysical characterization. The RED-labeled Target 1 sample showed acceptable labeling quality for TRIC measurements. In contrast, all ligand preparations showed some degree of solubility limitation after dilution into aqueous buffer (5% DMSO), emphasizing that downstream affinity analyses should be interpreted using clarified, experimentally determined working concentrations rather than nominal pre-centrifugation concentrations.

Target 1 QUALITY CONTROL AND ASSESSMENT OF DMSO COMPATIBILITY

Prior to ligand-binding studies, Target 1 was subjected to an orthogonal quality-control workflow consisting of SDS-PAGE, C), aSEC, and DSF to evaluate sample integrity, folding state, solution behavior, and thermal stability (**Figure 1**).

SDS-PAGE analysis demonstrated that Target 1 migrated as a single diffuse band with an apparent molecular weight (MW_{app}) of approximately 55 kDa (**Figure 1A-inset**). Although the theoretical molecular weight of the polypeptide is approximately ~27 kDa, the upward mobility shift and characteristic broad ("fuzzy") electrophoretic profile are consistent with glycosylation. No lower-molecular-weight degradation products or higher-molecular-weight species were detected, indicating that the purified material was intact and free of detectable proteolytic degradation.

Far-UV CD spectroscopy revealed a spectrum characterized by a pronounced negative minimum near 215–218 nm and the absence of the double minima at 208 and 222 nm typically associated with α-helical proteins. This spectral profile is consistent with a protein enriched in β-sheet secondary structure. The presence of a well-defined CD signal further confirms that the protein is folded under the experimental conditions employed (**Figure 1A**).

Analytical SEC demonstrated that Target 1 eluted predominantly as a single, symmetrical peak with an elution volume of 14.31 mL, indicating a largely monodisperse preparation with minimal aggregation. The estimated hydrodynamic radius (R_s) of approximately 2.43 nm and frictional ratio (f/f_0) of approximately 1.34 suggest a moderately elongated or glycosylated globular protein rather than a highly compact spherical particle (**Figure 1B**).

To establish assay-compatible DMSO concentrations, once that the ligands show high propensity for aggregation even at 5% DMSO, the thermal stability of Target 1 was evaluated by DSF in the presence of 0 to 5% DMSO (**Figure 1C and 1D**). All conditions exhibited a cooperative unfolding transition, demonstrating that the protein remained folded throughout the tested solvent range. However, increasing DMSO concentrations progressively reduced the melting temperature (T_m) of Target 1, indicating solvent-induced destabilization of the native state. The relationship between T_m and DMSO concentration was approximately linear over the tested range, resulting in an overall thermal destabilization of approximately -2 °C at 5% DMSO. Despite this effect, Target 1 retained a well-defined unfolding transition even at the highest DMSO concentration examined. These results indicate that the protein tolerates low DMSO concentrations commonly used in biophysical screening campaigns, while higher concentrations may negatively impact conformational stability and should therefore be minimized during ligand-binding experiments.

Collectively, the orthogonal QC data demonstrate that Target 1 is intact, properly folded, predominantly β-sheet in character, monodisperse in solution, and sufficiently stable for downstream biophysical characterization.

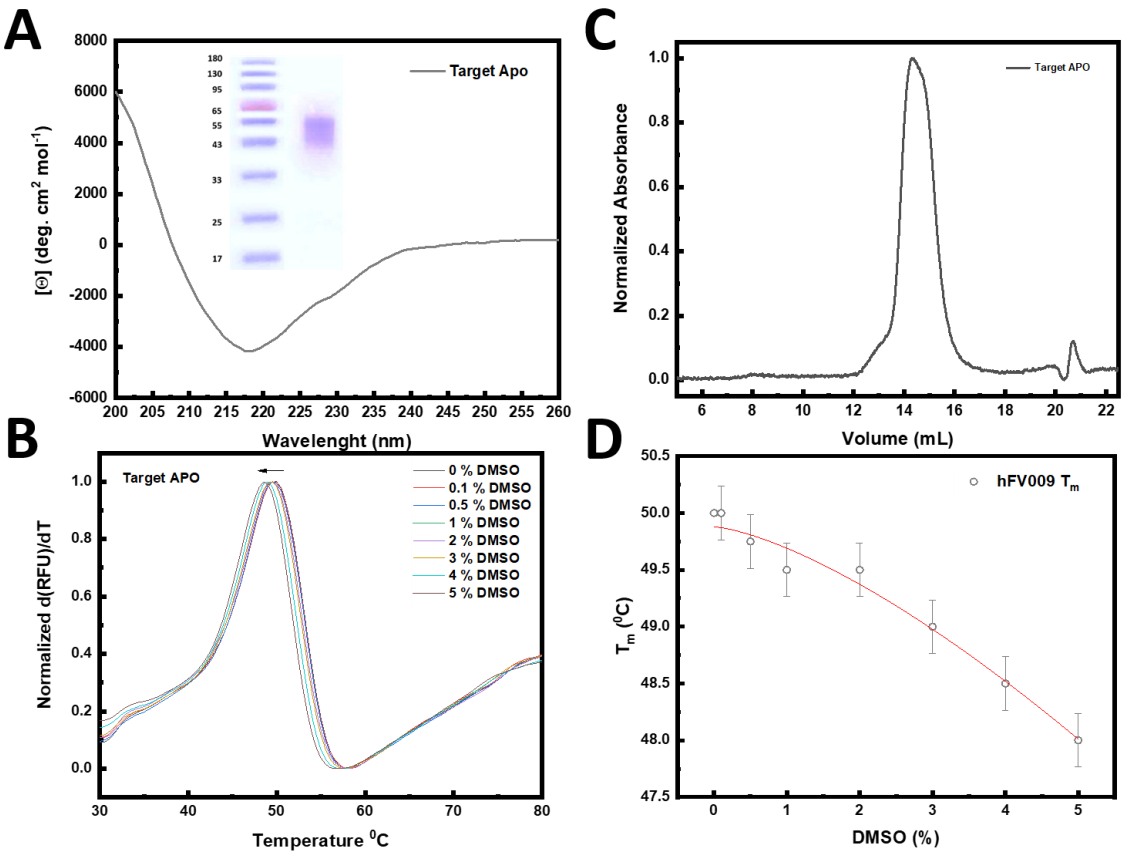

Figure 1. Orthogonal quality-control assessment of Target 1 and evaluation of DMSO-induced thermal destabilization. (A) Far-UV circular dichroism spectrum of Target 1 displaying a pronounced minimum near 216–218 nm, consistent with a protein enriched in β-sheet secondary structure and confirming that the protein is folded under the assay conditions employed. **(A-inset)** SDS-PAGE analysis of purified Target 1 showing a single predominant diffuse band with an apparent molecular weight (MW_{app}) of approximately 55 kDa. Although the theoretical molecular weight of Target 1 is ~27 kDa, the observed mobility shift and characteristic broad ("fuzzy") band are consistent with glycosylation. No evidence of significant degradation or high-molecular-weight aggregation was detected. **(B)** Analytical size-exclusion chromatography chromatogram showing a single dominant and symmetrical elution peak, indicating that Target 1 is predominantly monodisperse in solution with minimal aggregate/oligomers content. **(C)** Differential scanning fluorimetry thermal unfolding profiles collected in the presence of increasing DMSO concentrations (0–5% v/v). All conditions exhibited cooperative unfolding transitions, indicating retention of a folded protein population across the tested DMSO range. **(D)** Dependence of the melting temperature (T_m) on DMSO concentration. Increasing DMSO concentrations progressively reduced the thermal stability of Target 1, resulting in an overall decrease of approximately --2 °C between 0% and 5% DMSO. Despite this destabilization, Target 1 maintained a well-defined unfolding transition throughout the solvent range tested. Collectively, these orthogonal analyses demonstrate that Target 1 is intact, properly folded, predominantly monodisperse, and sufficiently stable for downstream biophysical characterization, while establishing acceptable DMSO concentrations for ligand-binding studies.

SDS-PAGE IN A PRESENCE OF LIGANDS

SDS-PAGE analysis was performed to evaluate the integrity of Target 1 following incubation with Ligand_1 and Ligand_2 (30 min). Under all conditions, Target 1 migrated as a single predominant diffuse band with an apparent molecular weight (MW_{app}) of approximately 55 kDa. Importantly, the electrophoretic profile remained unchanged following incubation with either Ligand_1 or Ligand_2. No evidence of ligand-induced proteolytic degradation, protein fragmentation, covalent modification, or formation of SDS-stable oligomeric species was detected. Likewise, no additional bands or changes in band intensity were observed in the presence of either ligand. These results indicate that Target 1 remains structurally intact following ligand exposure and that neither Ligand_1 nor Ligand_2 induces detectable alterations in protein integrity or electrophoretic behavior under the experimental conditions employed.

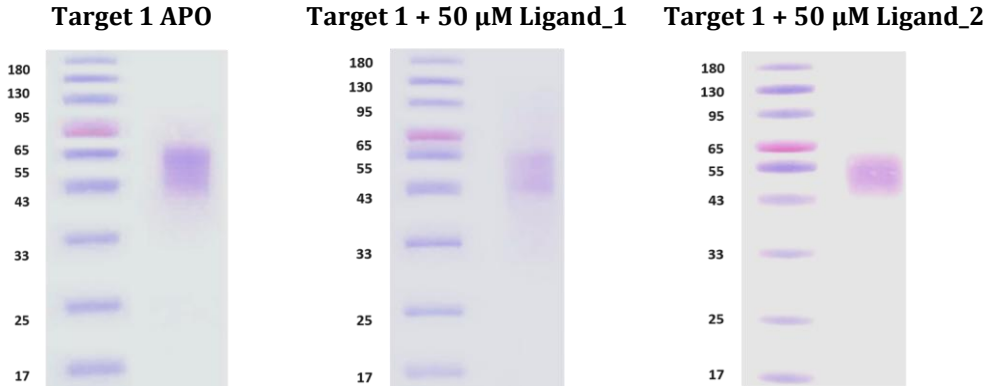

Figure 2. SDS-PAGE assessment of Target 1 integrity in the absence and presence of ligands. Purified Target 1 was analyzed by SDS-PAGE following incubation in the absence (apo) or presence of 50 µM Ligand_1 or 50 µM Ligand_2. Comparable electrophoretic profiles were observed under all conditions, with no detectable changes in migration behavior, protein fragmentation, degradation products, or high-molecular-weight species following ligand incubation. These results demonstrate that Ligand_1 or Ligand_2 adversely affects the integrity of Target 1 and confirms that the protein remained suitable for downstream biophysical characterization.

CIRCULAR DICHROISM ANALYSIS OF TARGET 1 IN THE PRESENCE OF LIGAND_1 AND LIGAND_2

Far-UV CD spectroscopy was used to evaluate whether ligand binding alters the secondary structure of Target 1. The apo protein exhibited a spectrum characterized by a pronounced negative minimum centered at approximately 2016-218 nm and the absence of the double minima at 208 and 222 nm typically associated with α-helical proteins (**Figure 3**). This spectral profile is consistent with a protein containing a substantial β-sheet component and confirms that Target 1 adopts a folded conformation under the experimental conditions employed.

Comparison of the apo Target 1 spectrum with spectra collected in the presence of 50 µM Ligand_1 or 50 µM Ligand_2 revealed nearly complete overlap across the entire wavelength range analyzed (200–260 nm). No significant changes in ellipticity, minimum wavelength position, or overall spectral shape were observed following ligand addition. The absence of measurable spectral perturbations indicates that neither ligand induces detectable alterations in the global secondary-structure content of Target 1.

These findings suggest that ligand binding does not promote large-scale conformational rearrangements, unfolding, or secondary-structure stabilization/destabilization detectable by far-UV CD. Consequently, any ligand-dependent effects observed in downstream biophysical assays are unlikely to arise from major changes in the overall fold of Target 1 and instead may reflect more localized structural or dynamic perturbations that are not resolved by CD spectroscopy.

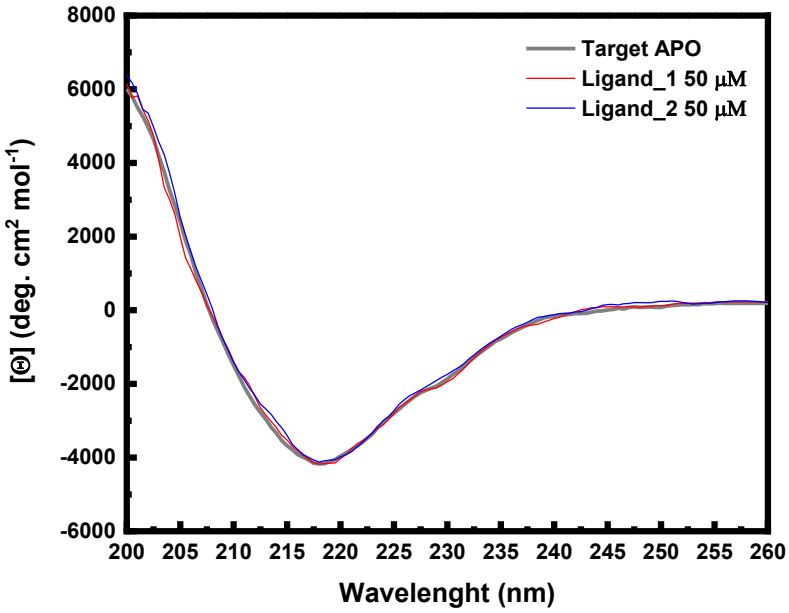

Figure 3. Far-UV circular dichroism analysis of Target 1 in the absence and presence of ligands. Far-UV CD spectra of Target 1 alone (black) and in the presence of 50 µM Ligand_1 (red) or 50 µM Ligand_2 (blue) were collected between 200 and 260 nm. The apo protein displays a characteristic minimum at approximately 216-218 nm, consistent with a protein enriched in β-sheet secondary structure. The spectra obtained in the presence of Ligand_1 and Ligand_2 are nearly superimposable with that of the apo protein, indicating that ligand binding does not produce detectable changes in the global secondary-structure content or overall fold of Target 1 under the experimental conditions employed. These results demonstrate that both ligands preserve the native structural integrity of Target 1 and do not induce significant conformational perturbations detectable by far-UV CD spectroscopy.

ANALYTICAL SIZE-EXCLUSION CHROMATOGRAPHY REVEALS A HOMOGENEOUS AND STRUCTURALLY STABLE TARGET 1 POPULATION IN SOLUTION

Analytical SEC was performed to evaluate the solution behavior of Target 1 and to determine whether Ligand_1 or Ligand_2 induce detectable changes in the hydrodynamic properties, oligomeric state, or aggregation profile of the protein (**Figure 4, Table 6**).

In the absence of ligand, Target 1 eluted as a single dominant and highly symmetrical peak with an elution volume (V_e) of 14.31 mL, indicating that the purified protein exists predominantly as a homogeneous and monodisperse species in solution. Notably, the chromatographic peak exhibited minimal broadening and no evidence of shoulder formation, suggesting a low degree of conformational heterogeneity despite the glycosylation observed by SDS-PAGE. Furthermore, no significant species were detected at lower elution volumes, indicating the absence of appreciable soluble higher-order oligomeric assemblies under the conditions employed.

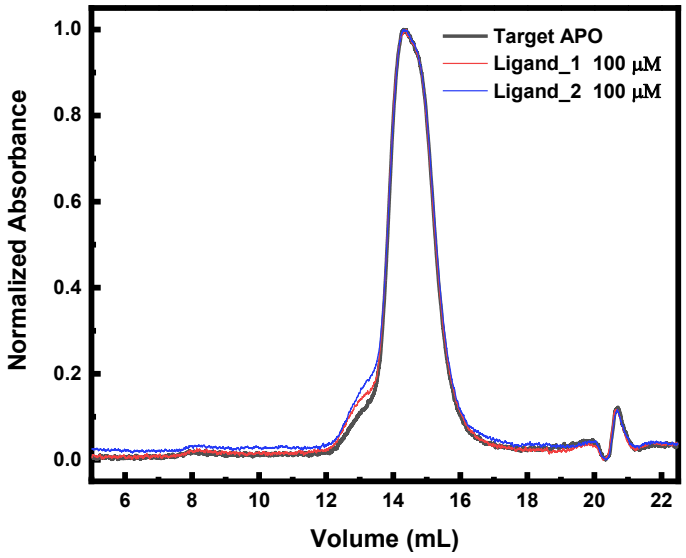

Figure 4. Analytical size-exclusion chromatography analysis of Target 1 in the absence and presence of ligands. Normalized aSEC chromatograms of apo Target 1 (black), Target 1 incubated with 100 µM Ligand_1 (red), and Target 1 incubated with 100 µM Ligand_2 (blue). All samples eluted as a single, symmetrical peak centered at approximately 14.3 mL, indicating that Target 1 exists predominantly as a homogeneous and monodisperse species in solution. The nearly complete overlap of the chromatographic profiles demonstrates that neither Ligand_1 nor Ligand_2 induces detectable changes in the hydrodynamic properties, oligomeric state, or aggregation behavior of Target 1. Consistent with the calculated hydrodynamic parameters (**Table 6**), ligand binding does not produce measurable alterations in the global size, shape, or conformational distribution of the protein under the conditions examined.

Incubation with either Ligand_1 or Ligand_2 produced chromatographic profiles that were nearly superimposable with that of the apo protein. The principal elution peak remained

highly symmetrical and retained essentially identical peak width, peak shape, and retention characteristics. No additional peaks corresponding to ligand-induced aggregation, oligomerization, dissociation, or degradation products were observed. Importantly, the complete overlap of the leading and trailing edges of the chromatographic peaks indicates that ligand binding does not measurably alter the conformational distribution of Target 1 in solution.

Quantitative analysis of the chromatographic data further supports the aforementioned conclusion (**Table 6**). The measured elution volumes varied by less than 0.1 mL across all conditions (14.31–14.37 mL), corresponding to nearly identical partition coefficients (K_{av} = 0.402–0.406). Similarly, the estimated hydrodynamic radii remained unchanged, ranging from approximately 2.40 to 2.43 nm, while the calculated frictional ratios (f/f_0 = 1.33–1.34) were indistinguishable within experimental uncertainty. These frictional ratios are consistent with a moderately asymmetric glycoprotein and agree with the apparent molecular properties observed by SDS-PAGE, where glycosylation resulted in an apparent molecular weight substantially greater than the theoretical polypeptide mass.

Collectively, the aSEC data demonstrate that Target 1 exists as a highly homogeneous and monodisperse protein population in solution. Neither Ligand_1 nor Ligand_2 induced detectable changes in molecular size, shape, conformational distribution, oligomeric state, or aggregation propensity. The remarkable overlap of the chromatographic profiles, together with the indistinguishable hydrodynamic parameters summarized in **Table 6**, indicates that ligand binding does not produce large-scale structural rearrangements or measurable alterations in the global solution properties of Target 1 under the conditions examined.

Table 6. Effect of Ligand Binding on the Hydrodynamic Properties of Target 1.

Sample	V_e	K_{av}	Est. R_s	Est. f/f_0
Target 1 APO	14.31 mL	0.402	~2.43 nm	~1.34
+ Ligand_1	14.37 mL	0.406	~2.40 nm	~1.33
+ Ligand_2	14.35 mL	0.404	~2.41 nm	~1.33

DIFFERENTIAL SCANNING FLUORIMETRY IDENTIFIES LIGAND_1 AND LIGAND_2 AS STABILIZING LIGANDS OF TARGET 1 AND ENABLES ESTIMATION OF APPARENT BINDING AFFINITY ($K_{D,APP}$)

DSF was employed to evaluate the effect of Ligand_1 and Ligand_2 on the thermal stability of Target 1 and to determine apparent binding affinities through ligand-dependent thermal stabilization analysis (**Figure 5**).

In the absence of ligand, Target 1 exhibited a single, well-defined unfolding transition characteristic of a structurally homogeneous protein population. Addition of either Ligand_1 or Ligand_2 shifted the unfolding transition toward higher temperatures,

demonstrating stabilization of the native protein state upon ligand binding. Importantly, both ligands produced a substantial rightward displacement of the melting transition while preserving the overall shape and cooperativity of the unfolding profile.

The derivative melting curves remained monophasic under all conditions, with no evidence of peak splitting, broadening, or secondary unfolding events. These observations indicate that ligand binding stabilizes the native conformational ensemble of Target 1 without generating detectable structural heterogeneity or alternative thermodynamic populations. Furthermore, the absence of additional transitions suggests that neither ligand promotes aggregation, partial unfolding, or formation of distinct ligand-bound conformational states detectable by DSF.

To quantify ligand binding, thermal stabilization was measured across a range of ligand concentrations and analyzed using a saturation binding model. Both compounds produced clear concentration-dependent increases in thermal stability that approached a common saturation plateau, consistent with specific and saturable binding interactions. The resulting datasets were exceptionally well described by the fitted models, yielding coefficients of determination (R^2) of 0.998 for Ligand_1 and 0.9974 for Ligand_2.

Analysis of the stabilization curves yielded apparent dissociation constants ($K_{D,app}$) of approximately 4 μM for Ligand_1 and 8 μM for Ligand_2. These results indicate that Ligand_1 binds Target 1 with approximately two-fold greater apparent affinity than Ligand_2. Notably, despite this difference in affinity, both ligands achieved similar maximal stabilization responses at saturating concentrations, suggesting that they stabilize a comparable conformational state of Target 1 once full target occupancy is reached.

The combination of pronounced thermal stabilization, saturable dose-response behavior, low-micromolar apparent affinities, and excellent model fits provides strong evidence for direct ligand engagement. Collectively, these data identify Ligand_1 and Ligand_2 as bona fide binders of Target 1 and demonstrate that ligand binding results in substantial stabilization of the folded protein. Among the compounds tested, Ligand_1 emerged as the more potent ligand, exhibiting the highest apparent affinity and the most efficient stabilization of Target 1.

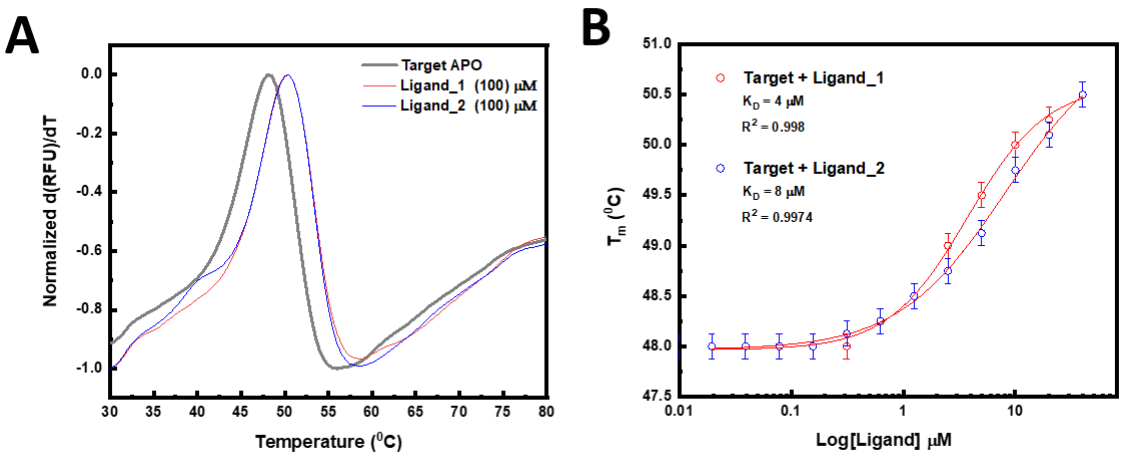

Figure 5. Differential scanning fluorimetry demonstrates ligand-dependent stabilization of Target 1 by Ligand_1 and Ligand_2. (A) First-derivative DSF melting curves of Target 1 in the absence (black) and presence of 40 µM Ligand_1 (red) or Ligand_2 (blue). Both ligands shifted the thermal unfolding transition toward higher temperatures relative to the apo protein, indicating stabilization of the native state upon ligand binding. The unfolding profiles remained monophasic and highly cooperative under all conditions, with no evidence of secondary transitions, peak broadening, or structural heterogeneity, suggesting that ligand binding stabilizes the native conformational ensemble without inducing detectable alternative folding states. **(B)** Concentration-dependent thermal stabilization of Target 1 measured by DSF. Increasing concentrations of Ligand_1 and Ligand_2 produced saturable increases in protein stability consistent with specific ligand binding. Nonlinear regression analysis yielded apparent dissociation constants ($K_{D,app}$) of approximately 4 µM for Ligand_1 and 8 µM for Ligand_2, with excellent agreement between experimental data and fitted binding models (R^2 = 0.998 and 0.9974, respectively). Although both ligands achieved similar maximal stabilization at saturation, Ligand_1 exhibited approximately two-fold higher apparent affinity, identifying it as the more potent stabilizer of Target 1 under the conditions examined. Collectively, these data provide strong evidence for direct ligand engagement and demonstrate that both compounds stabilize the folded state of Target 1 through specific binding interactions.

TRIC CONFIRMS DIRECT BINDING OF LIGAND_1 AND LIGAND_2 TO TARGET 1

Target engagement was further evaluated using temperature-related intensity change measurements. Both Ligand_1 and Ligand_2 produced clear concentration-dependent changes in the TRIC signal, demonstrating direct interaction with Target 1 (**Figure 6**).

Increasing ligand concentration resulted in progressive decreases in normalized fluorescence intensity (ΔF_{norm}), generating well-defined sigmoidal binding curves that approached saturation at high ligand concentrations. The observed responses were highly reproducible across the concentration range examined and were consistent with a specific and saturable binding process. Importantly, both ligands reached similar maximal response amplitudes at saturation, suggesting that Ligand_1 and Ligand_2 ultimately stabilize or perturb a similar protein conformational state once full target occupancy is achieved.

Nonlinear regression analysis yielded equilibrium dissociation constants ($K_{D,app}$) of approximately 4 µM for Ligand_1 and 7 µM for Ligand_2, with excellent agreement between the fitted models and the experimental data (R^2 = 0.9906 and 0.9981, respectively). These results indicate that Ligand_1 binds Target 1 with modestly higher affinity than Ligand_2, consistent with the leftward shift observed in the binding isotherm.

Notably, the affinities determined by TRIC closely agree with those independently obtained by DSF-based thermal stabilization experiments ($K_{D,app}$ ≈ 4 µM and 8 µM, respectively). The convergence of these values across two orthogonal biophysical techniques provides strong evidence that the measured interactions are specific and experimentally robust. Furthermore, the absence of biphasic binding behavior, anomalous curvature, or concentration-dependent signal distortions suggests that binding is dominated by a single interaction event within the concentration range examined.

Collectively, the TRIC data confirm direct binding of both Ligand_1 and Ligand_2 to Target 1 and independently validate the rank order of affinity observed by DSF. Among the compounds tested, Ligand_1 consistently displayed the highest affinity, whereas Ligand_2 exhibited slightly weaker but readily measurable target engagement.

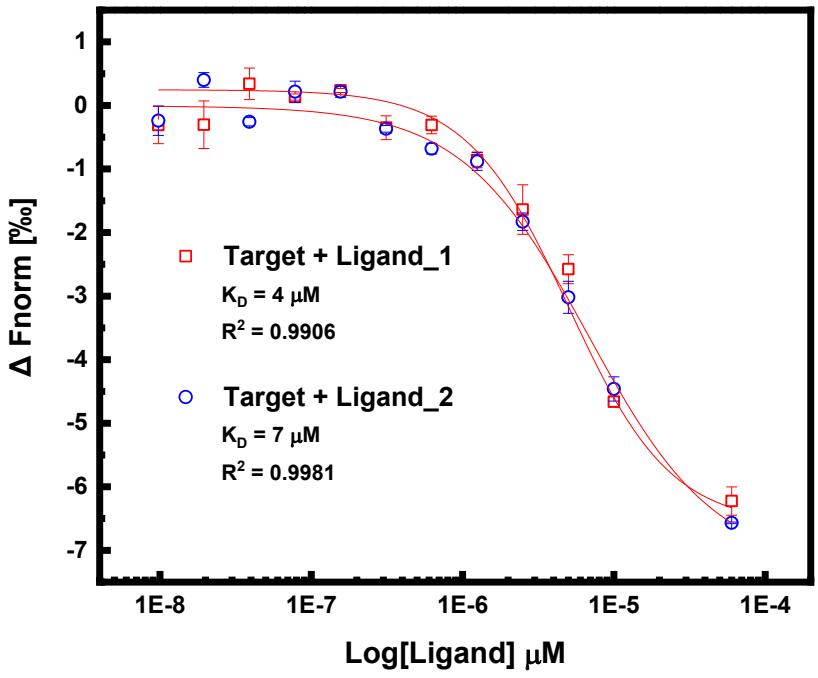

Figure 6. TRIC analysis of Target 1 binding to Ligand_1 and Ligand_2. Normalized TRIC responses (ΔF_{norm}) were measured as a function of ligand concentration and fitted using a one-site binding model. Ligand_1 (red) and Ligand_2 (blue) produced concentration-dependent and saturable changes in the TRIC signal, demonstrating direct interaction with Target 1. Nonlinear regression yielded equilibrium dissociation constants ($K_{D,app}$) of approximately 4 µM for Ligand_1 and 7 µM for Ligand_2, with excellent goodness-of-fit values (R^2 = 0.9906 and 0.9981, respectively). Both ligands reached similar maximal response amplitudes at saturation, indicating comparable effects on the local environment of the labeled protein. The close

agreement between TRIC- and DSF-derived affinities provides orthogonal confirmation of ligand binding and identifies Ligand_1 as the higher-affinity ligand under the conditions examined.

FLUORESCENCE POLARIZATION CONFIRMS SPECIFIC BINDING OF LIGAND_1-ALEXA643 AND LIGAND_2-ALEXA643 TO TARGET 1

FP was employed as an orthogonal solution-phase binding assay to evaluate the interaction of the fluorescent tracers Ligand_1-alexa643 and Ligand_2-alexa643 with Target 1. Both ligands produced clear concentration-dependent increases in fluorescence polarization upon titration with Target 1, consistent with formation of protein–ligand complexes and the corresponding reduction in rotational mobility of the fluorescent tracers (**Figure 7**).

The binding curves exhibited the characteristic sigmoidal behavior expected for a saturable molecular recognition process and were exceptionally well described by a single-site binding model. Ligand_1-alexa643 displayed a left-shifted binding isotherm relative to Ligand_2-Alexa643, indicating higher affinity for Target 1. Nonlinear regression analysis yielded apparent dissociation constants ($K_{D,app}$) of approximately 3 μM for Ligand_1-Alexa643 and 7 μM for Ligand_2-alexa643, with excellent goodness-of-fit values (R^2 = 0.99915 and 0.99967, respectively). These results demonstrate that both fluorescent tracers retain robust target-binding capability following labeling and purification.

Importantly, no measurable concentration-dependent FP response was observed when either tracer was incubated with lysozyme, which served as a negative protein control. The absence of signal generation in the control experiments demonstrates that the observed polarization changes are not driven by nonspecific interactions with protein surfaces, fluorescence artifacts, or tracer self-association. Instead, the response is specific to Target 1, providing strong evidence that the measured FP signal arises from bona fide target engagement, at least when compared with lysozyme.

A second independently analyzed FP dataset yielded nearly identical binding parameters, producing $K_{D,app}$ values of approximately 3 μM and 7 μM for Ligand_1-alexa643 and Ligand_2-Alexa643, respectively, with similarly excellent fit statistics. The high degree of agreement between independent analyses highlights the reproducibility and robustness of the FP measurements.

The affinity ranking observed by FP is fully consistent with the orthogonal DSF and TRIC datasets. Across all three techniques, the Ligand_1/Ligand_1-Alexa643 ligand series consistently exhibited higher affinity for Target 1 than the Ligand_2/Ligand_2-Alexa643 series. Furthermore, the absolute affinity values determined by FP closely match those obtained from DSF-based thermal stabilization experiments and TRIC binding measurements, despite the fundamentally different physical principles underlying each technique. Such convergence across orthogonal methodologies substantially increases confidence in the measured affinities and strongly supports the conclusion that both ligands engage Target 1 through specific binding interactions.

Notably, UV-visible quality-control analysis performed prior to the FP studies revealed significant loss of soluble material during ligand preparation, with approximately 43% of both Ligand_1-Alexa643 and Ligand_2-Alexa643 removed following centrifugation due to precipitation or aggregation. Despite this reduction in ligand concentration, both tracers generated highly reproducible binding curves with excellent fit quality, indicating that the remaining soluble fractions were chemically intact and fully competent for target recognition. Taken together, these results identify Ligand_1-Alexa643 and Ligand_2-Alexa643 as specific Target 1 binders and provide independent validation of the affinity ranking established by DSF and TRIC.

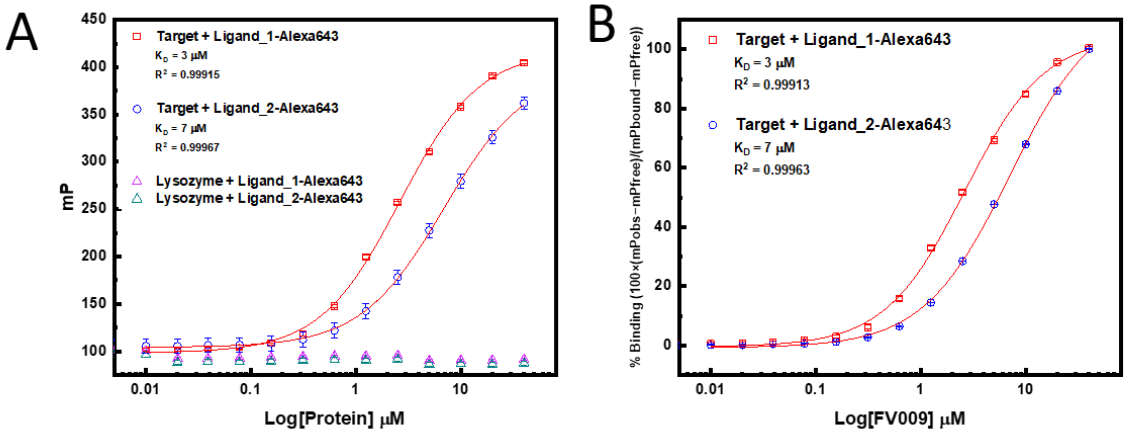

Figure 7. Fluorescence polarization analysis of fluorescent ligand binding to Target 1. (A) Fluorescence polarization binding curves mP versus Log[protein] and **(B)** % Binding versus Log[protein] were generated by titrating Target 1 against the fluorescent ligands Ligand_1-Alexa643 and Ligand_2-Alexa643. Both ligands produced concentration-dependent and saturable increases in FP signal, consistent with formation of Target 1–ligand complexes. Ligand_1-Alexa643 showed a left-shifted binding curve and higher apparent affinity, with $K_{D,app} \approx 3$ µM, whereas Ligand_2-Alexa643 bound with $K_{D,app} \approx 7$ µM. Excellent fit quality was obtained for both ligands, with R^2 values ≥ 0.999. Lysozyme controls **(A)** showed no concentration-dependent FP response, supporting the specificity of the interaction with Target 1. The repeated analysis produced the same affinity ranking and comparable K_D values, confirming the reproducibility of the FP-derived binding constants.

SURFACE PLASMON RESONANCE CONFIRMS SPECIFIC BINDING AND DEFINES THE KINETIC MECHANISM OF LIGAND RECOGNITION

Surface plasmon resonance was employed to directly characterize the interaction between Target 1 and the lead ligands under solution conditions identical to those used throughout the orthogonal biophysical workflow. Single-cycle kinetic experiments generated concentration-dependent sensorgrams for both compounds that were well described by a global 1:1 Langmuir binding model (**Figure 8**). In contrast, buffer injections produced essentially flat sensorgrams with responses remaining at baseline throughout the association and dissociation phases, demonstrating negligible nonspecific binding, minimal bulk refractive-index effects, and appropriate reference subtraction.

Both Ligand_1 and Ligand_2 exhibited rapid concentration-dependent association followed by measurable dissociation after completion of the injection phase. Increasing ligand concentrations produced progressively larger responses that approached saturation without evidence of heterogeneous binding behavior, secondary kinetic phases, or concentration-dependent deviations from the fitted model. The close agreement between the experimental sensorgrams and the global kinetic fits indicates that the interactions are adequately described by a single dominant binding event under the experimental conditions employed.

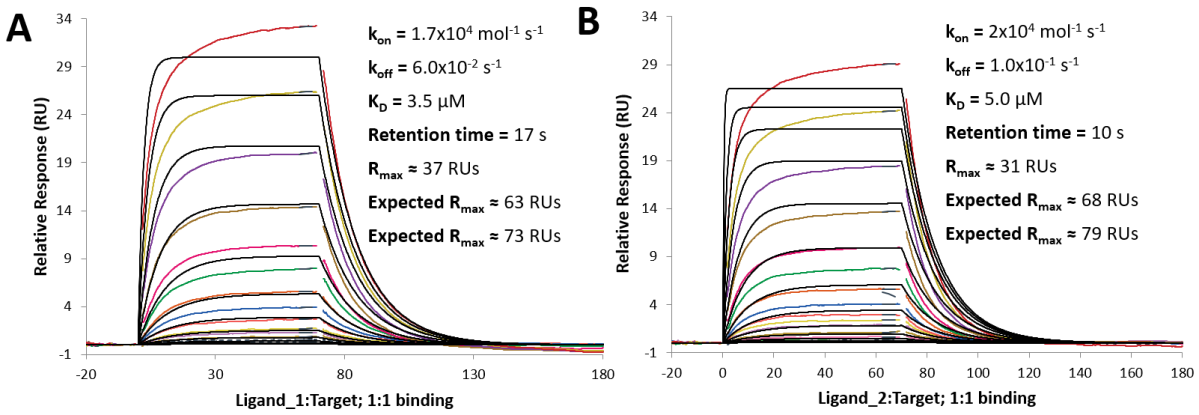

Figure 8. Surface plasmon resonance (SPR) kinetic analysis of Ligand_1 and Ligand_2 binding to Target 1. Representative single-cycle kinetic (SCK) sensorgrams for **(A)** Ligand_1 and **(B)** Ligand_2 interacting with immobilized Target 1. Colored traces represent the experimental sensorgrams obtained using increasing ligand concentrations, whereas the black lines correspond to the global fits generated using a 1:1 Langmuir binding model. Both ligands exhibited concentration-dependent association followed by measurable dissociation, consistent with specific molecular recognition. Ligand_1 displayed slower dissociation and higher equilibrium responses than Ligand_2, indicating the formation of a more kinetically stable complex and greater target occupancy under identical experimental conditions. Global kinetic analysis yielded apparent equilibrium dissociation constants (K_D) of approximately 3.5 µM for Ligand_1 and 5.0 µM for Ligand_2, consistent with Ligand_1 exhibiting the stronger interaction with Target 1.

Global kinetic analysis demonstrated that Ligand_1 binds Target 1 with a higher apparent affinity than Ligand_2. Ligand_1 exhibited an apparent equilibrium dissociation constant (K_D) of approximately 3.5 µM, whereas Ligand_2 bound with an apparent K_D of approximately 5.0 µM. The improved affinity of Ligand_1 was driven primarily by its slower dissociation rate and longer residence time, indicating formation of a more kinetically stable Target 1–ligand complex relative to Ligand_2 (k_{on} = 1.7 × 10^4 M^{-1} s^{-1}) and a slower dissociation rate (k_{off} = 6.0 × 10^-2 s^{-1}) compared with Ligand_2 (k_{on} = 2.0 × 10^4 M^{-1} s^{-1}, k_{off} = 1.0 × 10^{-1} s^{-1}), yielding a longer residence time on the target (~17 s versus ~10 s, respectively). These results indicate that the Ligand_1 complex is kinetically more stable following target engagement.

Maximum binding responses reached approximately 37 RU for Ligand_1 and 31 RU for Ligand_2. Although these responses were lower than the theoretical R_{max} values predicted from the immobilization level, both compounds displayed highly reproducible

concentration-dependent binding with well-defined saturation behavior, demonstrating that the immobilized protein remained functionally active throughout the experiment.

Because Ligand_1 and Ligand_2 possess nearly identical molecular weights, differences in SPR response cannot be attributed to analyte mass. Instead, the measured equilibrium responses were used to estimate the relative occupancy of the immobilized Target 1 surface. Under identical experimental conditions, Ligand_1 achieved approximately 30% greater target occupancy than Ligand_2, indicating that a substantially larger fraction of the available binding sites was occupied by Ligand_1 at equivalent ligand concentrations. This independent occupancy analysis is fully consistent with the higher affinity determined by kinetic analysis and further supports superior target engagement by Ligand_1.

Steady-state equilibrium analysis (**Figure 9**) provided independent affinity estimates that closely supported the kinetic analysis. Fitting the equilibrium response as a function of ligand concentration yielded apparent dissociation constants of approximately 1.6 µM for Ligand_1 and 7.8 µM for Ligand_2, with excellent goodness-of-fit values (R^2 = 0.996 and 0.997, respectively). Although the absolute K_D values obtained from steady-state and kinetic analyses differed modestly, both approaches consistently identified Ligand_1 as the higher-affinity ligand and produced the same rank order of target binding.

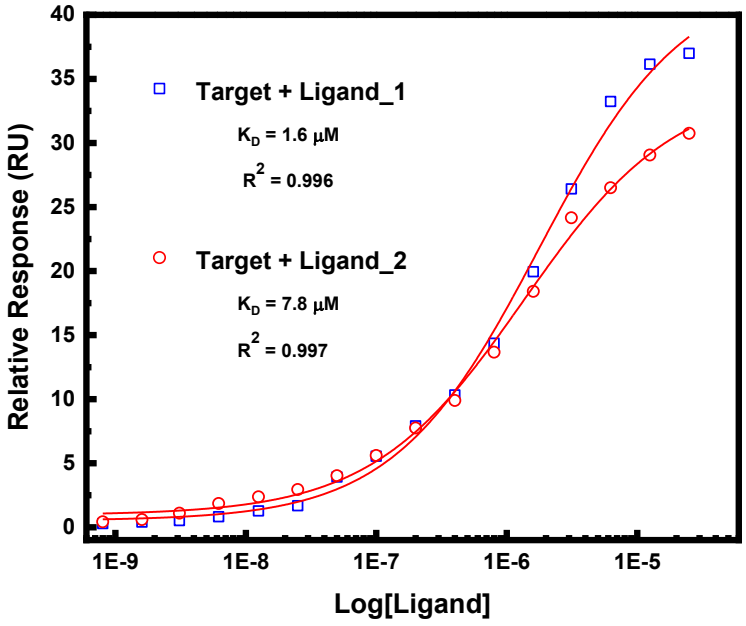

Figure 9. Steady-state SPR analysis independently confirms the higher affinity of Ligand_1 for Target 1. Equilibrium binding responses measured by surface plasmon resonance were plotted as a function of ligand concentration and fitted using a one-site steady-state binding model. Ligand_1 (blue squares) and Ligand_2 (red circles) both exhibited concentration-dependent and saturable binding, demonstrating specific interaction with immobilized Target 1. Steady-state analysis yielded apparent equilibrium dissociation constants (K_D) of approximately 1.6 µM for Ligand_1 and 7.8 µM for Ligand_2, with excellent goodness-of-fit values (R^2 = 0.996 and 0.997, respectively). At saturating ligand concentrations, Ligand_1 produced a

substantially greater equilibrium response than Ligand_2. Because both ligands possess nearly identical molecular weights, the higher response observed for Ligand_1 reflects approximately 30% greater target occupancy under identical experimental conditions. The steady-state analysis independently confirms the affinity ranking obtained from kinetic SPR measurements, identifying Ligand_1 as the higher-affinity ligand and demonstrating superior target engagement relative to Ligand_2.

Importantly, the affinity ranking determined by SPR is fully consistent with the orthogonal biophysical measurements obtained by DSF, TRIC, fluorescence polarization, and ITC. Across all independent techniques, Ligand_1 reproducibly exhibited stronger interaction with Target 1 than Ligand_2, while the negative-control buffer injections showed no measurable response. The convergence of kinetic, equilibrium, occupancy, fluorescence-based, thermal-stability, and calorimetric measurements provides compelling evidence that both ligands specifically engage Target 1, with Ligand_1 consistently demonstrating superior target binding under the experimental conditions examined.

ISOTHERMAL TITRATION CALORIMETRY

ITC was employed to provide direct thermodynamic characterization of ligand binding to Target 1 and to serve as an orthogonal validation of the affinity measurements obtained by SPR, TRIC, MST, FP, and DSF. Because both compounds displayed substantial solubility limitations and required 5% DMSO to remain in solution, a series of control experiments was first performed to determine whether the calorimetric signals observed during protein titrations could be confidently attributed to molecular recognition rather than instrumental artifacts, solvent effects, or compound dilution phenomena.

Instrument Qualification and Assay Controls

The first control consisted of water-to-water injections **(Figure 10A)**. This experiment was performed to evaluate baseline stability, injection reproducibility, thermal equilibration, and the overall performance of the calorimeter under conditions where no measurable binding or dilution heat is expected. The resulting thermogram displayed a stable baseline with small and highly reproducible injection artifacts, demonstrating that the instrument was operating under thermally stable conditions and that the injection system was functioning reproducibly throughout the experiment.

A second control involved titration of $CaCl_2$ into buffer **(Figure 10B)**. This experiment was designed to evaluate heat contributions arising solely from injection, mixing, and dilution. Under these conditions, no specific binding event occurs, and therefore the measured heat should approach zero. The negligible heat observed throughout the titration demonstrated that the calorimetric response of the instrument was not dominated by dilution artifacts and established a baseline expectation for a non-binding experiment.

Finally, $CaCl_2$ was titrated into EDTA **(Figure 10C)**. Unlike the previous controls, this experiment represents a well-characterized, strongly exothermic binding interaction with an expected stoichiometry of approximately 1:1. The resulting thermogram displayed the

characteristic sharp transition associated with a high-affinity interaction and yielded a fitted stoichiometry of N = 0.95. This experiment served as a positive control, demonstrating that the instrument could accurately detect, integrate, and fit a genuine molecular recognition event. Importantly, the observed transition occurred near the expected molar ratio of one, confirming accurate syringe delivery and proper calorimetric performance.

Together, these three controls established that the calorimeter exhibited stable baseline behavior, minimal dilution artifacts, and the ability to accurately detect a known binding event. Consequently, subsequent heat signals observed during ligand titrations could be interpreted with confidence as arising from interactions between the compounds and Target 1.

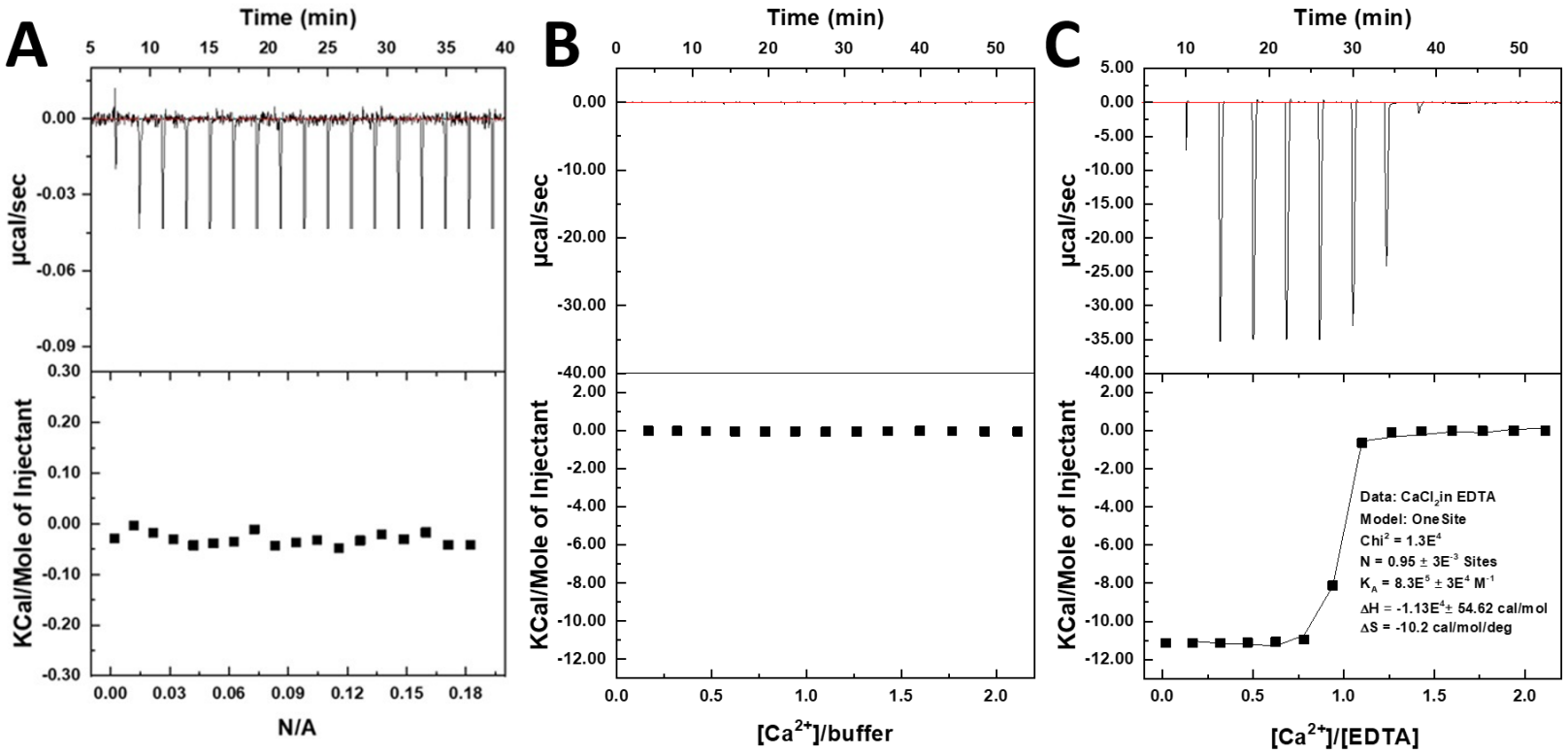

Figure 10. ITC instrument qualification and control titrations. (A) Water-to-water injections were performed to evaluate baseline stability, injection reproducibility, and thermal equilibration of the ITC instrument in the absence of binding or dilution heat. The small and consistent injection artifacts indicate stable instrument performance. **(B)** $CaCl_2$ titrated into buffer was used to assess heat from injection, dilution, and mixing in the absence of a binding partner. Minimal heat was observed, indicating negligible $CaCl_2$ dilution heat under the assay conditions. **(C)** $CaCl_2$ titrated into EDTA served as a positive control for heat-producing molecular recognition. The titration produced a strong exothermic transition near a molar ratio of one with N = 0.95, confirming proper injection delivery, peak integration, and detection of a known 1:1 binding event. The fitted affinity is not interpreted as the true Ca^{2+}–EDTA K_D because the interaction is too tight for accurate KD determination under these conditions.

Ligand Dilution Heat Controls

Because both Ligand_1 and Ligand_2 required elevated DMSO concentrations to maintain solubility and exhibited evidence of concentration-dependent aggregation during sample preparation, ligand-to-buffer control experiments were performed to quantify heat contributions arising from compound dilution, solvent mixing, and potential aggregation-related effects in the absence of protein. These experiments were essential for distinguishing true binding signals from calorimetric responses associated solely with the compounds themselves.

Titration of Ligand_1 into buffer produced only small dilution heats throughout the experiment (**Figure 11A**). The resulting thermogram displayed low-amplitude injection signals and a stable baseline, indicating that dilution of the compound generated minimal heat under the experimental conditions employed. Similarly, Ligand_2 produced relatively small dilution heats (**Figure 11B**); however, a modest increase in baseline noise was observed relative to Ligand_1. This behavior is consistent with the more challenging solubility characteristics of Ligand_2 and likely reflects increased susceptibility to aggregation or microheterogeneity in solution. Importantly, despite these differences, the magnitude of the dilution heat remained substantially smaller than the calorimetric signals observed during titration into Target 1.

These control experiments demonstrate that neither compound generated sufficient dilution heat to explain the binding isotherms observed in the presence of protein. Furthermore, the relatively small magnitude of the ligand-to-buffer signals indicates that solvent mixing and compound dilution contributed only minimally to the total heat measured during the protein titrations. Consequently, the calorimetric responses observed in the presence of Target 1 can be primarily attributed to ligand-protein interactions rather than compound-associated artifacts.

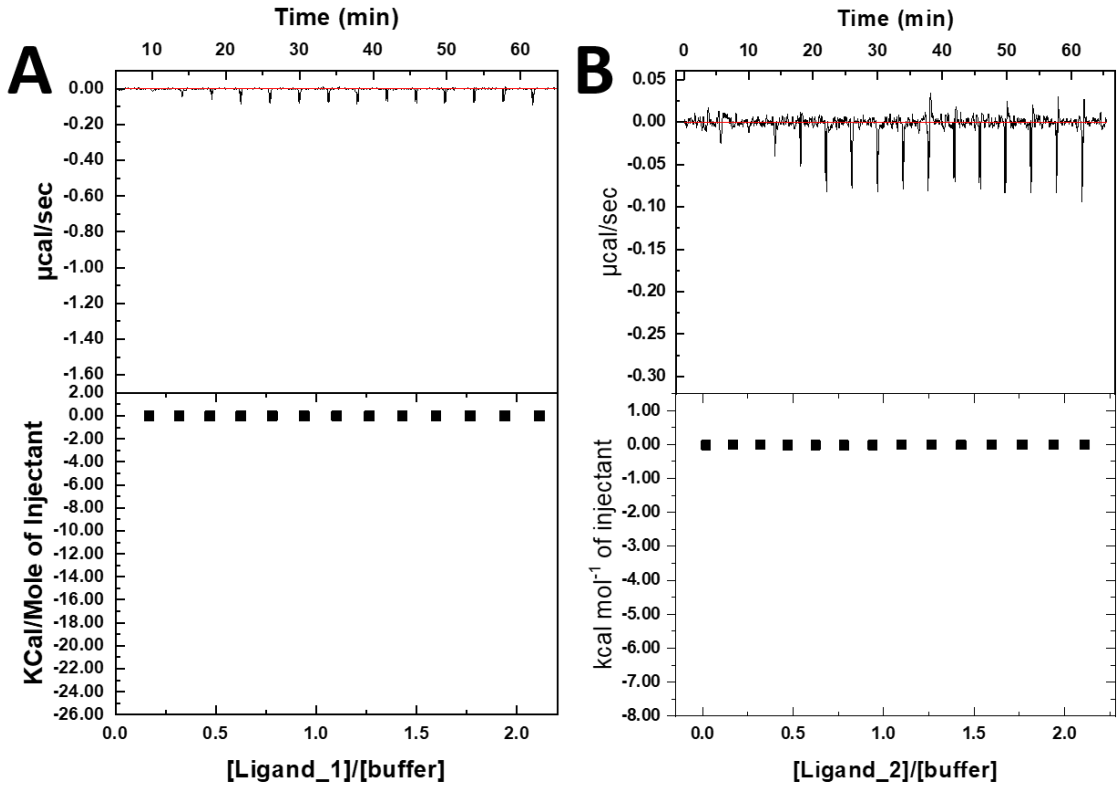

Figure 11. Ligand-to-buffer dilution controls. (A) Ligand_1 titrated into buffer produced only small dilution heats, indicating minimal compound-associated heat in the absence of Target 1. **(B)** Ligand_2 titrated into buffer produced modest injection-associated signals and slightly higher baseline noise, consistent with more challenging compound behavior. In both cases, the dilution heats were substantially smaller than the heats observed during titration into Target 1, supporting that the protein titration signals primarily reflect ligand binding rather than DMSO mismatch, dilution heat, or compound-only artifacts.

Thermodynamic Characterization of Ligand_1 and Ligand_2 Binding to Target 1

Following instrument qualification and ligand-control experiments, ITC was used to directly characterize the interaction of Ligand_1 and Ligand_2 with Target 1 (**Figure 12**). Both compounds produced saturable exothermic binding isotherms consistent with specific molecular recognition. The observed heat signals were substantially larger than those measured in the ligand-to-buffer controls and displayed characteristic binding transitions that could be adequately described using a one-site binding model.

Titration of Ligand_1 into Target 1 generated a well-defined exothermic binding isotherm with a fitted stoichiometry of N = 0.91, indicating an interaction approaching a 1:1 binding ratio. Analysis of the integrated binding heats yielded an apparent dissociation constant ($K_{D,app}$) of approximately 3.4 µM. Thermodynamic analysis revealed a strongly favorable enthalpic contribution (ΔH = −25.4 kcal/mol) accompanied by a substantial unfavorable entropic contribution (−TΔS = +17.9 kcal/mol), resulting in an overall binding free energy of approximately ΔG = −7.5 kcal/mol. These results indicate that binding of Ligand_1 is

predominantly driven by favorable intermolecular interactions, while conformational restriction, desolvation effects, or other entropy-reducing processes partially oppose complex formation.

Ligand_2 likewise produced a saturable exothermic binding isotherm and a fitted stoichiometry of N = 0.99, indicating essentially ideal 1:1 binding behavior. The fitted apparent dissociation constant was approximately 6.5 μM, indicating weaker binding relative to Ligand_1. The thermodynamic signature was qualitatively similar, with binding driven by a favorable enthalpic contribution (ΔH = −22.5 kcal/mol) and opposed by an unfavorable entropic contribution (−TΔS = +15.4 kcal/mol), resulting in an overall binding free energy of approximately ΔG = −7.1 kcal/mol. The similarity of the thermodynamic profiles suggests that both compounds engage Target 1 through a common binding mechanism and likely interact with similar regions of the target protein.

Comparison of the thermodynamic parameters revealed that Ligand_1 possesses a modest affinity advantage over Ligand_2. This difference appears to arise primarily from a more favorable enthalpic contribution rather than substantial differences in overall binding free energy. Such behavior is consistent with two structurally related ligands that engage a common binding site but differ slightly in the strength or number of favorable intermolecular contacts formed upon binding.

Several limitations should be considered when interpreting the ITC-derived affinity values. Both compounds displayed substantial solubility limitations, requiring the use of 5% DMSO and preventing preparation of ligand concentrations typically preferred for optimal ITC analysis. Significant compound aggregation was observed during sample preparation, reducing the maximum achievable soluble ligand concentration. Consequently, the ligand-to-protein concentration ratios used in the experiments were lower than ideal, and the post-transition regions of the binding isotherms were not fully extended. Under optimized conditions, higher ligand concentrations would provide improved saturation and more robust determination of equilibrium and thermodynamic parameters. For this reason, the affinities reported herein are considered apparent dissociation constants (K_D,app) that reflect the experimental conditions under which the measurements were performed.

Despite these limitations, the ITC results provide compelling evidence of direct molecular recognition. Both compounds produced saturable binding isotherms with stoichiometries near unity, thermodynamic signatures characteristic of specific binding, and apparent affinities that were highly consistent with independent measurements obtained by SPR, TRIC, MST, FP, and DSF. The convergence of these orthogonal biophysical techniques strongly supports direct binding of Ligand_1 and Ligand_2 to Target 1 and establishes that both interactions are predominantly enthalpy-driven under the experimental conditions employed.

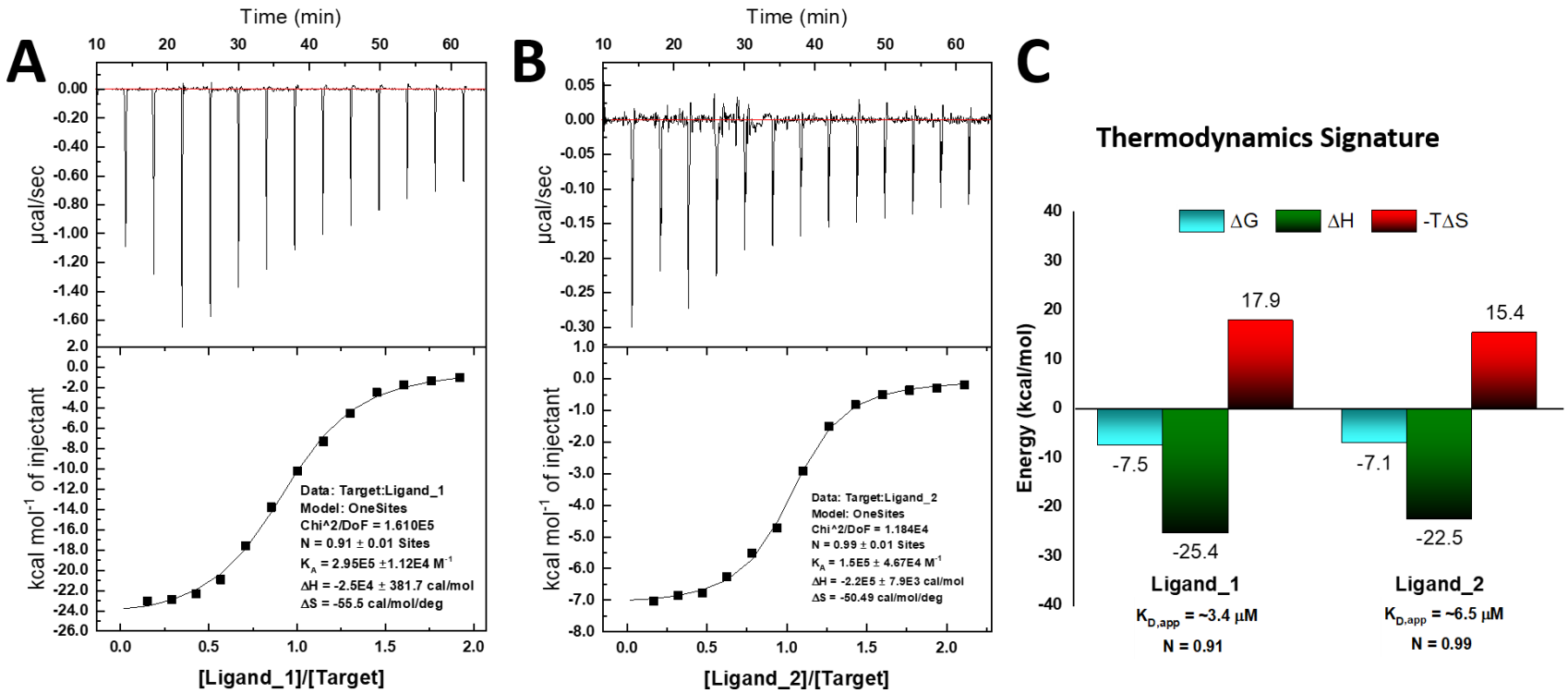

Figure 12. Thermodynamic characterization of Ligand_1 and Ligand_2 binding to Target 1 by ITC. (A) Titration of Ligand_1 into Target 1 produced a saturable exothermic binding isotherm. Fitting to a one-site model yielded $K_{D,app} \approx 3.4$ µM and N = 0.91. **(B)** Titration of Ligand_2 into Target 1 also produced a saturable exothermic binding isotherm, yielding $K_{D,app} \approx 6.5$ µM and N = 0.99. **(C)** Thermodynamic decomposition of binding free energy showed that both ligands bind through favorable enthalpic contributions partially offset by unfavorable entropic terms. Ligand_1 displayed ΔG = −7.5 kcal/mol, ΔH = −25.4 kcal/mol, and −TΔS = +17.9 kcal/mol, while Ligand_2 displayed ΔG = −7.1 kcal/mol, ΔH = −22.5 kcal/mol, and −TΔS = +15.4 kcal/mol. Due to ligand solubility limitations and the requirement for 5% DMSO, ITC-derived affinities are reported as apparent dissociation constants.

DISCUSSION

Successful hit validation extends well beyond demonstrating a measurable interaction in a single assay. Each biophysical technique interrogates a distinct physical property of the protein–ligand system and is therefore susceptible to different experimental limitations, assay-specific artifacts, and sources of uncertainty. Consequently, confidence in molecular recognition is maximized when multiple orthogonal methodologies converge on the same biological conclusion despite relying on fundamentally different physical principles. The present study was therefore designed as an integrated orthogonal biophysical characterization workflow in which protein quality, structural integrity, solution behavior, thermal stability, binding kinetics, target occupancy, and thermodynamic properties were independently evaluated before being interpreted collectively.

The first objective of this study was to determine whether Target 1 represented a suitable substrate for quantitative biophysical characterization. This question is frequently underestimated during early discovery campaigns, yet protein quality remains one of the largest contributors to experimental uncertainty. A partially unfolded, heterogeneous, unstable, or aggregated protein can generate misleading affinity measurements regardless of the analytical platform employed. For this reason, the study began with an orthogonal quality-control workflow integrating SDS-PAGE, circular dichroism, analytical size-exclusion chromatography, and differential scanning fluorimetry.

Collectively, these experiments demonstrate that Target 1 is an intact, properly folded, predominantly β-sheet glycoprotein that exists as a highly homogeneous and monodisperse population in solution. SDS-PAGE confirmed the absence of detectable degradation or higher-order species despite the expected mobility shift associated with glycosylation. Circular dichroism demonstrated preservation of the native secondary structure, whereas analytical SEC revealed a single symmetrical chromatographic peak with unchanged hydrodynamic parameters. Differential scanning fluorimetry further showed that although increasing DMSO concentrations progressively reduced thermal stability by approximately -2°C, the protein maintained a cooperative unfolding transition even in the presence of 5% DMSO. Together, these observations substantially reduce uncertainty regarding protein quality and establish that all subsequent ligand-binding measurements were performed using a structurally intact and assay-compatible protein preparation.

An equally important outcome of the quality-control workflow was the identification of ligand solubility, not protein instability, as the principal experimental limitation encountered throughout the study. UV-visible spectroscopic analysis demonstrated that all ligands experienced significant losses in soluble material following dilution into aqueous buffer, despite the presence of 5% DMSO. Aggregation increased markedly in the absence of 0.05% Tween-20, indicating that the physicochemical properties of the compounds, rather than the target protein, imposed the primary limitation on quantitative affinity determination. This distinction is critical because it establishes that the experimental constraints observed during ITC and high-concentration binding experiments originated from compound behavior instead of deficiencies in the protein preparation.

Perhaps the most important observation emerging from this study is the remarkable convergence obtained across every orthogonal technique employed. Despite measuring fundamentally different physical observables, including protein integrity, secondary structure, hydrodynamic behavior, thermal stability, fluorescence response, binding kinetics, equilibrium occupancy, and calorimetric heat release, all methods support a single, internally consistent mechanistic model. Target 1 remains structurally intact throughout ligand binding, while both compounds specifically recognize and stabilize the native conformational ensemble without inducing detectable large-scale structural rearrangements. This degree of agreement substantially increases confidence that the observed interactions represent genuine molecular recognition rather than assay-dependent artifacts.

Interestingly, the structural techniques reveal what ligand binding does not do. Neither SDS-PAGE, circular dichroism, nor analytical SEC detected measurable alterations in protein integrity, secondary structure, molecular dimensions, oligomeric state, or conformational distribution following ligand binding. The nearly superimposable CD spectra indicate preservation of the global β-sheet architecture, while identical chromatographic profiles, Stokes radii, and frictional ratios demonstrate that ligand association does not produce detectable conformational expansion, compaction, oligomerization, or aggregation. These observations strongly suggest that ligand recognition occurs without remodeling the overall protein architecture.

Conversely, the functional biophysical techniques reveal what ligand binding does accomplish. Differential scanning fluorimetry demonstrated that both compounds increased the melting temperature of Target 1 by approximately 2.5°C while preserving a single cooperative unfolding transition. The absence of peak broadening, secondary

unfolding events, or multiple thermodynamic populations indicates that ligand binding stabilizes the existing native conformational ensemble rather than inducing alternative folded states. The identical maximal thermal stabilization produced by both ligands further suggests that each compound ultimately stabilizes essentially the same structural state once high target occupancy is achieved.

The direct binding assays provide additional mechanistic resolution. TRIC, fluorescence polarization, SPR, and ITC independently confirmed specific molecular recognition and consistently ranked Ligand_1 as the higher-affinity ligand. Remarkably, although each technique measures a different physical property, the apparent affinities cluster within the same low-micromolar range, providing unusually strong orthogonal validation. Such agreement across fluorescence-based, thermal, kinetic, equilibrium, and calorimetric methodologies is rarely observed unless the underlying interaction is both robust and highly reproducible.

Among all techniques employed, SPR provides the greatest mechanistic insight because it separates equilibrium affinity into its kinetic components. While both compounds display comparable overall binding behavior and follow a simple 1:1 interaction model, Ligand_1 consistently forms the more kinetically stable complex. Specifically, SPR demonstrates a slower dissociation rate, a longer residence time, higher equilibrium responses, and approximately 30% greater target occupancy under identical experimental conditions. Importantly, because both ligands possess nearly identical molecular weights, the higher SPR response cannot be attributed to analyte mass but instead reflects occupation of a larger fraction of functional binding sites on the immobilized protein.

When interpreted together, the SPR data suggests that the primary distinction between the two compounds is not whether they bind, but rather how effectively the resulting complex is stabilized following initial target engagement. Although definitive assignment of the binding site requires high-resolution structural methods such as X-ray crystallography or cryo-electron microscopy, the remarkable agreement among CD, aSEC, DSF, SPR, and ITC strongly supports a model in which Ligand_1 and Ligand_2 recognize the same or highly overlapping binding interface on Target 1. Both ligands preserve the global secondary structure, hydrodynamic properties, oligomeric state, and thermodynamic stoichiometry of the protein while producing nearly identical thermal stabilization, indicating that they engage the same native conformational ensemble. In contrast, the principal differences emerge only in the kinetic parameters measured by SPR, where Ligand_1 displays slower dissociation, longer residence time, and approximately 30% greater target occupancy.

Collectively, these observations make alternative binding sites or fundamentally different binding mechanisms less parsimonious than a model in which both ligands occupy the same binding pocket but differ in the quality and persistence of the intermolecular interactions established within that interface.

The thermodynamic measurements reinforce this interpretation. ITC demonstrated that both interactions are strongly enthalpy-driven and opposed by unfavorable entropy, with nearly identical stoichiometries approaching one ligand per protein molecule. Such thermodynamic signatures are consistent with formation of numerous favorable non-covalent interactions, including hydrogen bonds, electrostatic contacts, and van der Waals interactions, accompanied by conformational restriction and solvent reorganization upon complex formation. Importantly, the slightly more favorable enthalpy observed for Ligand_1 parallels its superior kinetic behavior measured by SPR, suggesting that the longer residence time arises from optimization of a limited number of local intermolecular interactions rather than from a fundamentally different binding mechanism.

This interpretation has important implications for medicinal chemistry. The integrated dataset provides little evidence that future optimization should focus on discovering an entirely different chemotype or binding mode. Instead, the data indicate that the existing scaffold already achieves productive molecular recognition while preserving the native structural properties of the target. Consequently, future SAR efforts are more likely to benefit from optimization of the protein–ligand interface rather than wholesale scaffold redesign. Structural modifications that strengthen hydrogen-bond persistence, improve hydrophobic complementarity, reduce local solvent accessibility, or restrict ligand conformational flexibility may preferentially decrease the dissociation rate, thereby increasing residence time and target occupancy without altering the overall binding mechanism.

This distinction is particularly relevant because equilibrium affinity alone does not fully describe pharmacologically relevant target engagement. Two ligands possessing similar equilibrium affinities may exhibit substantially different biological performance if one remains associated with the target for longer periods. The present study illustrates this principle clearly. Although Ligand_1 and Ligand_2 display comparable structural effects and broadly similar affinities across orthogonal techniques, Ligand_1 consistently exhibits longer residence time and greater target occupancy. These kinetic advantages suggest that optimization of dissociation kinetics may represent a more productive direction for future SAR than attempts to improve equilibrium affinity alone.

Several limitations should nevertheless be considered when interpreting the quantitative affinity measurements. Significant ligand aggregation restricted the maximum soluble concentrations available for several experiments, particularly ITC, and necessitated the use of 5% DMSO to maintain partial solubility. Consequently, complete saturation of the calorimetric binding isotherms could not be achieved under ideal experimental conditions, and the ITC-derived affinities are therefore most appropriately interpreted as apparent dissociation constants. Likewise, the lower-than-theoretical SPR responses likely reflect the fraction of immobilized protein that remained functionally accessible following surface immobilization rather than deviations from the proposed binding model. Importantly, these limitations influence the precision of the numerical affinity estimates but do not alter the central biological conclusions because every orthogonal technique independently reaches the same affinity ranking and mechanistic interpretation.

Overall, the integrated biophysical dataset supports a coherent mechanistic model in which Ligand_1 and Ligand_2 specifically recognize the same native conformational state of Target 1 without inducing detectable global structural rearrangements. Ligand binding stabilizes the existing folded ensemble while preserving protein integrity, secondary structure, oligomeric state, and solution behavior. The principal distinction between the compounds resides not in the mechanism of molecular recognition but in the quality and persistence of the intermolecular interactions formed within the binding interface. Ligand_1 consistently exhibits slower dissociation, longer residence time, greater target occupancy, and higher affinity across multiple independent techniques, indicating formation of a kinetically more stable protein–ligand complex. From a medicinal chemistry perspective, these observations suggest that future optimization should prioritize strengthening the existing interaction network responsible for reducing the dissociation rate rather than redesigning the overall binding scaffold. The remarkable agreement among orthogonal structural, kinetic, equilibrium, fluorescence-based, and thermodynamic measurements substantially reduces experimental uncertainty and provides a robust framework for structure–activity relationship development, rational lead optimization, and future functional characterization of Target 1 ligands.

CONCLUSIONS

This study provides a comprehensive orthogonal biophysical characterization of Target 1 and establishes a high-confidence framework for interpreting ligand binding through the integration of complementary structural, kinetic, thermodynamic, and solution-based methodologies. Rather than relying on a single experimental endpoint, molecular recognition was independently evaluated using SDS-PAGE, circular dichroism, analytical size-exclusion chromatography, differential scanning fluorimetry, TRIC, fluorescence polarization, surface plasmon resonance, and isothermal titration calorimetry. The remarkable agreement among these fundamentally different techniques substantially reduces experimental uncertainty and provides compelling evidence that the conclusions presented here reflect genuine molecular recognition rather than assay-specific artifacts.

Prior to ligand characterization, Target 1 was demonstrated to be an intact, properly folded, predominantly β-sheet, monodisperse, and assay-compatible protein suitable for quantitative biophysical studies. Although elevated DMSO concentrations produced a modest reduction in thermal stability, the protein remained structurally competent under all assay conditions required for ligand evaluation. Importantly, the principal experimental limitation encountered throughout this work originated from ligand solubility and aggregation rather than deficiencies in protein quality, ensuring that the observed binding behavior reflects authentic target–ligand interactions.

Independent orthogonal measurements unequivocally demonstrate that both Ligand_1 and Ligand_2 directly engage Target 1 with low-micromolar affinity. Across DSF, TRIC, fluorescence polarization, SPR, and ITC, both compounds consistently exhibited saturable and specific binding while preserving the native structural and solution properties of the protein. Neither ligand induced detectable alterations in protein integrity, secondary structure, oligomeric state, or hydrodynamic behavior, indicating that molecular recognition occurs without disrupting the global architecture of Target 1. Instead, both ligands stabilize the native conformational ensemble, as evidenced by a reproducible increase of approximately 2.5°C in protein thermal stability.

Among the compounds evaluated, Ligand_1 consistently emerged as the superior ligand. Although both compounds appear to recognize the same native protein state and produce nearly identical structural and thermodynamic consequences, SPR revealed that Ligand_1 forms a more kinetically stable complex characterized by slower dissociation, longer residence time, and approximately 30% greater target occupancy under identical

experimental conditions. These observations strongly suggest that the improved performance of Ligand_1 arises from optimization of the molecular interface rather than engagement of an alternative binding mechanism. Consequently, the current scaffold appears to represent a productive starting point for medicinal chemistry, with future structure–activity relationship (SAR) efforts likely benefiting from optimization of intermolecular contacts that further reduce the dissociation rate and extend target residence time rather than from wholesale scaffold redesign.

The thermodynamic analysis further demonstrated that binding of both ligands is predominantly enthalpy-driven, indicating that favorable intermolecular interactions, including hydrogen bonding, electrostatic contacts, and van der Waals complementarity, are the principal contributors to molecular recognition. While compound solubility prevented acquisition of fully optimized calorimetric isotherms, the convergence of ITC with SPR, DSF, TRIC, and fluorescence polarization confirms that these experimental limitations affect only the precision of the numerical affinity estimates and do not alter the fundamental biological conclusions.

Collectively, the present work establishes that Target 1 is a robust and biophysically tractable target suitable for ligand-discovery and lead-optimization efforts. Ligand_1 and Ligand_2 are validated Target 1 binders supported by multiple independent lines of experimental evidence, while Ligand_1-Alexa643 and Ligand_2-Alexa643 are validated fluorescent tracers suitable for future target-engagement, competition, and screening assays. Most importantly, the integrated dataset provides a clear mechanistic framework to guide medicinal chemistry: preserve the current binding mode while optimizing molecular interactions that enhance kinetic stability and target residence time. This strategy offers the greatest opportunity to improve target engagement while maintaining the favorable structural and biophysical properties demonstrated throughout this study.

Taken together, this work delivers considerably more than quantitative affinity measurements. It provides a rigorous, orthogonally validated understanding of how these ligands interact with Target 1, identifies the molecular features that distinguish the current lead compounds, and establishes a strong experimental foundation for rational SAR optimization, structural studies, functional validation, and subsequent stages of lead development. In this context, Ligand_1 should be considered the primary chemical starting point for continued optimization, with Ligand_2 serving as a valuable comparator for defining the structural determinants governing affinity, residence time, and productive target engagement.

The integrated orthogonal strategy employed in this study substantially reduces the probability of false-positive or assay-specific conclusions, providing a high level of confidence for subsequent medicinal chemistry decision-making.

MATERIALS

Protein

Protein Target 1 provided by client ***(1 mg total)***

Table 7. Protein Molecular Identity and Physicochemical Properties.

Property	Target 1 (target)
Number of amino acids	236
Molecular Weight (Da)	26138.34
Extinction Coefficient (ε280) (M^{-1} cm^{-1})	25690
Isoelectric Point (pI)	5.71
Oligomeric State	Monomer
Glycosylation Status	2 glycosylation sites
Construct Boundaries	N/A
Tags	polyhistidine tag at the C-terminus
Expression System	human 293 cells (HEK293)
Quality control (SDS-PAGE)	The protein has a calculated MW of 26.4 kDa. The protein migrates as 39-55 kDa when calibrated against Star Ribbon Pre-stained Protein Marker under reducing (R) condition (SDS-PAGE) due to glycosylation
Quality control (SEC-Malls)	The purity of Target 1, His Tag is more than 95% and the molecular weight of this protein is around 35-53 kDa verified by SEC-MALS
Quality control (Bioactivity-ELISA)	Immobilized Target 1, His Tag at 2 μg/mL (100 μL/well) can bind Anti-body MAb (Human IgG1) with a linear range of 0.2-6 ng/mL (QC tested)
Purification Tag(s)	polyhistidine tag at the C-terminus
Reducing Agent Requirement	N/A
Cofactor Requirement	N/A
Metal Dependency	N/A
Buffer Compatibility	20 mM Hepes (pH=7.4), 150 mM NaCl, 0.05% Tween20 and 5% DMSO (max) (TESTED IN THIS REPORT)
Thermal Stability (T_m)	Nd
Solubility Range	Vendor highly advises to keep protein at a higher concentration of 1 mg/mL (about 37 μM).
Aggregation Tendency	Aggregates in presence of some ligands (not checked concentration dependency)
Storage Conditions	Storage at -80 C
Freeze-Thaw Stability	Highly recommend avoid Freeze-Thaw cycles
Concentration Range for Studies	Vendor highly advises keep protein at a higher concentration of 1 mg/mL (about 37 μM).
Intrinsic Fluorescence Content (Trp/Tyr)	Protein has: 3 W and 6 Y.
Known Ligands	Ligand_1, Ligand_2, Ligand_1-Alexa643 and Ligand_2-Alexa643

Known Binding Affinity Range	K_D is in a range of 50 to 5000 nM by SPR
Functional State Requirements	Protein must be monomeric, monodisperse and preserve secondary and tertiary structures.
Propension to aggregation	Protein Aggregates in the presence of some ligands

Ligands

Ligand_1, Ligand_2, Ligand_1-Alexa643 and Ligand_2-Alexa643 *(provided by client)*

Table 8. Ligand Molecular Identity and Physicochemical Properties

Property	Ligand_1	Ligand_2	Ligand_1-Alexa643	Ligand_2-Alexa643
Molecular Weight (Da)	1946.382	1960.409	3061.74	3075.767
Molecular Formula	N/A	N/A	N/A	N/A
Extinction Coefficient (ε280) (M^{-1} cm^{-1})	5625	5625	5625	5625
Isoelectric Point (pI)	6.01	6.01	5.58	5.58
Chemical Structure	N/A	N/A	N/A	N/A
SMILES/InChI	N/A	N/A	N/A	N/A
Solubility (water)	N/A	N/A	N/A	N/A
Solubility (assay buffer)	Soluble at 5% DMSO at 100 µM	Soluble at 5% DMSO at 100 µM	Soluble at 5% DMSO at 100 µM	Soluble at 5% DMSO at 100 µM
LogP/cLogP	-3.5	-3.3	-16.4	-16.4
LogD (pH 7.4)	-3.5	-3.3	-16.6	-16.4
PKa	14.4	14.4	N/A	N/A
pKa (acid)	6.6	6.6	N/A	N/A
pKa (basic)	14.4	14.4	N/A	N/A
Net Charge at Assay pH	N/A	N/A	N/A	N/A
Polar Surface Area (PSA)	683.9	683.9	1013.4	1013.4
Hydrogen Bond Donors	27	27	34	34
Hydrogen Bond Acceptors	43	43	65	65
Chemical Stability	N/A	N/A	N/A	N/A

METHODS

Protein preparation

The recombinant protein Target 1 was diluted to a final concentration of 0.7 mg/mL and subjected to overnight dialysis at 4°C against 1 L of buffer containing 20 mM HEPES (pH 7.4) and 150 mM NaCl. Following dialysis, the sample was centrifuged at 15,000 rpm for 30 min at 4°C. The supernatant was carefully collected and used for subsequent analyses.

Protein concentration was determined by UV absorbance at 280 nm using a NanoDrop spectrophotometer (Thermo Fisher Scientific). Concentrations were calculated using the molar extinction coefficient (ε_{280}) provided by the client.

Protein Quality Assessment

Following dialysis and concentration determination, the protein sample was visually inspected for evidence of precipitation, turbidity, or phase separation. No visible precipitation was observed following centrifugation, and only the clarified supernatant was used for subsequent experiments.

Ligand preparation

Ligands were received from the client as 10 mM stock solutions. Prior to analysis, each ligand was diluted to 500 µM in assay buffer containing 20 mM HEPES (pH 7.4) and 150 mM NaCl (final DMSO concentration of 5%).

Following dilution, ligand solutions were centrifuged at 15,000 rpm for 30 min at 4°C. The supernatants were carefully collected and used for subsequent experiments.

Ligand concentrations were determined by UV absorbance spectroscopy using a NanoDrop spectrophotometer (Thermo Fisher Scientific). Concentrations were calculated using the molar extinction coefficient (ε_{280}) provided by the client.

Ligand Quality Assessment

Ligand solutions were visually inspected before and after centrifugation for evidence of precipitation, turbidity, or insoluble material. Only clarified supernatants were used for downstream biophysical analyses.

NOTE: Protein and ligand solutions were prepared in identical buffer conditions (20 mM HEPES, pH 7.4, 150 mM NaCl) to minimize artifacts arising from buffer mismatch during downstream biophysical characterization.

Experimental Conditions, Instrument Parameters, and Data Analysis Procedures for Orthogonal Biophysical Characterization

Table 9. Experimental Conditions, Instrument Parameters, and Data Analysis Procedures for Orthogonal Biophysical Characterization.

Technique	Method
SDS-PAGE	Sodium dodecyl sulfate polyacrylamide gel electrophoresis (SDS-PAGE) was performed to evaluate protein integrity following ITC titrations. Samples analyzed included apo protein recovered from the buffer-to-protein control titration and protein recovered from ligand-to-protein titrations. Aliquots were mixed with 4× Laemmli sample buffer containing SDS with and without DTT, heated at 95°C for 5 min, and loaded onto 12% Mini-PROTEAN TGX precast polyacrylamide gels (Bio-Rad) together with a molecular weight standard. Electrophoresis was performed using a Bio-Rad Mini-PROTEAN Tetra Cell system in 1× Tris-Glycine-SDS running buffer at 180 V until adequate band separation was achieved. Following electrophoresis, gels were stained with Coomassie Brilliant Blue and destained in water. Protein banding patterns were compared between apo and ligand-treated samples to evaluate potential ligand-induced effects on protein integrity, including degradation, fragmentation, precipitation, covalent modification, or changes in sample purity.
CD	Circular dichroism (CD) spectroscopy was performed to evaluate the impact of ligand binding on the secondary structure and conformational stability of Target 1 following ITC experiments. Samples analyzed included the apo protein recovered from the buffer-to-protein control titration and the protein recovered from ligand-to-protein titrations. Ligand concentrations used in the ITC experiments were selected to achieve approximately 90% target occupancy, based on the estimated dissociation constants (K_D) obtained during preliminary biophysical characterization. Occupancy was calculated using the equilibrium binding equation and the final ligand concentration present in the ITC cell following completion of the titration. CD spectra were collected using a Jasco J-1500 Circular Dichroism Spectrometer equipped with a temperature-controlled cell holder. Measurements were performed at 25°C using a 0.1 cm pathlength quartz cuvette. Far-UV spectra were acquired from 190 to 260 nm with a data pitch of 1 nm, scan speed of 50 nm/min, response time of 1 s, and bandwidth of 1 nm. Multiple accumulations were averaged for each sample to improve signal-to-noise ratio. Buffer spectra were collected under identical conditions and subtracted from the corresponding protein spectra. Spectra obtained for apo and ligand-bound samples were compared to assess potential ligand-induced changes in protein secondary structure, conformational stability, folding state, or structural integrity. Particular attention was given to changes in spectral shape, ellipticity minima, and overall signal intensity that could indicate alterations in α-helical or β-sheet content resulting from ligand binding. Ligand concentrations were selected to achieve an estimated target occupancy of approximately 90%, calculated using the experimentally determined K_D values according to the equilibrium binding relationship: $$\textbf{Occupancy}\ (\%) = \frac{[\boldsymbol{L}]}{([\boldsymbol{L}] + \boldsymbol{KD}) * \mathbf{100}}$$ where [L] corresponds to the final free ligand concentration present in solution. **NOTE:** For CD DMSO concentrations were lower than 0.04% (assay limitation)
aSEC	Analytical size-exclusion chromatography (aSEC) was performed to evaluate the effect of ligand binding on the oligomeric state, hydrodynamic behavior, and sample homogeneity of Target 1 following ITC experiments. Samples analyzed included the apo protein recovered from the buffer-to-protein control titration and the protein recovered from ligand-to-protein titrations. Ligand concentrations used during the ITC experiments were selected to achieve approximately 90% target occupancy, based on the estimated dissociation constants (K_D) obtained during preliminary biophysical characterization. Occupancy was calculated using the equilibrium binding relationship and the final ligand concentration present in the ITC cell following titration. Prior to analysis, samples were centrifuged to remove any particulate material. A total volume of 100 µL was injected into a Superdex 200 Increase 10/300 GL column (Cytiva) equilibrated in running buffer containing 20 mM HEPES (pH 7.4), 150 mM NaCl, 3% DMSO, and 0.05% Tween-20. Chromatography was performed using an ÄKTA Pure FPLC system (Cytiva) at 25°C and a flow rate of 0.5 mL/min. Protein elution was monitored by UV absorbance at 280 nm. Chromatograms obtained for apo and ligand-bound samples were compared to assess potential ligand-induced effects on protein behavior, including changes in apparent molecular size, oligomerization state, aggregation, dissociation, conformational expansion or compaction, and overall sample

	monodispersity. Particular attention was given to shifts in elution volume, peak broadening, peak asymmetry, and the appearance of higher- or lower-molecular-weight species that could indicate ligand-induced alterations in protein quaternary structure or solution behavior. To further characterize ligand-induced structural effects, the Stokes radius (Rs) of each species was calculated from the experimentally determined elution volume using a column calibration curve generated with protein standards of known hydrodynamic properties. The resulting hydrodynamic radius values were subsequently used to estimate the frictional ratio (f/f_0) according to: $$f/f_0 = \frac{R_s}{R_0}$$ where R_s is the experimentally determined Stokes radius and R_0 is the radius of a hydrated sphere having the same molecular mass as the protein. Frictional ratio analysis was used to evaluate potential ligand-induced changes in molecular shape and compactness. Increases in f/f_0 were interpreted as evidence of a more extended or asymmetric molecular conformation, whereas decreases in f/f_0 were interpreted as evidence of structural compaction. Comparisons between apo and ligand-bound samples allowed assessment of whether ligand binding altered the global hydrodynamic properties of Target 1 independently of changes in oligomeric state. These analyses were used in conjunction with CD, DSF, TRIC, FP, and ITC data to establish a comprehensive view of the structural and biophysical consequences of ligand binding.
DSF	Differential scanning fluorimetry (DSF) was performed using a Bio-Rad CFX384 real-time PCR instrument and 384-well white PCR plates optimized for low-volume measurements. Thermal unfolding was monitored using SYPRO Orange dye (Thermo Fisher Scientific), which exhibits increased fluorescence upon binding to hydrophobic regions exposed during protein unfolding. All experiments were performed in a final buffer consisting of 20 mM HEPES (pH 7.4), 150 mM NaCl, 3% DMSO, and 0.05% Tween-20. Prior to ligand-binding studies, a DMSO tolerance experiment was conducted to identify the maximum DMSO concentration compatible with protein stability and assay performance. Protein samples were incubated with increasing concentrations of DMSO and analyzed by thermal unfolding to identify conditions that maintained a well-defined melting transition while minimizing solvent-induced destabilization. For ligand-binding studies, Target 1 was incubated with serial dilutions of each ligand to generate concentration-response curves. Samples were prepared at a final volume of 8 µL per well and allowed to equilibrate prior to thermal analysis. Thermal unfolding was monitored from 25°C to 95°C using a continuous temperature ramp while fluorescence was recorded throughout the experiment. Melting temperatures (T_m) were determined from the maximum of the first derivative of the fluorescence unfolding curves. Ligand binding was evaluated by comparison of the melting temperature of ligand-treated samples with the apo protein control. Positive binding events were identified by reproducible concentration-dependent shifts in melting temperature (ΔT_m). Apparent dissociation constants ($K_{D,app}$) were estimated by plotting ΔTm as a function of ligand concentration and fitting the resulting dose-response curves to a one-site saturation binding model: $$\Delta T_m = \Delta T_{m,max} \frac{[L]}{K_{D,app} + [L]}$$ where ΔT_m is the observed thermal stabilization, $\Delta T_{m,max}$ is the maximum thermal stabilization observed at saturating ligand concentrations, [L] is the ligand concentration, and $K_{D,app}$ represents the ligand concentration required to achieve half-maximal thermal stabilization. Apparent K_D values obtained from DSF were used for compound ranking and to estimate ligand concentrations required to achieve approximately 90% target occupancy in subsequent orthogonal biophysical assays.
TRIC	Temperature-Related Intensity Change (TRIC) measurements were performed using a Dianthus NT.23 instrument (NanoTemper Technologies) operated in plate-reader mode using the TRIC detector exclusively. TRIC was used as an orthogonal solution-phase binding assay to evaluate direct target engagement between Target 1 and the test ligands and to determine apparent equilibrium dissociation constants ($K_{D,app}$). Prior to analysis, Target 1 was fluorescently labeled using the Protein Labeling Kit RED-NHS 2nd Generation (NanoTemper Technologies) according to the manufacturer's protocol. Briefly, purified protein was exchanged into the labeling buffer supplied with the kit to remove primary amine-containing components that could interfere with the NHS ester reaction. The protein was subsequently mixed with the RED-NHS dye and incubated according to the manufacturer's recommendations, allowing covalent attachment of the fluorophore to accessible primary amines. Following completion of the labeling reaction, excess free dye was removed using the

	desalting columns provided with the kit. Protein concentration, fluorophore concentration, and degree of labeling were determined spectrophotometrically according to the manufacturer's instructions. Labeled protein preparations exhibiting acceptable labeling efficiency and fluorescence intensity were used for subsequent TRIC experiments. For binding studies, labeled Target 1 was diluted in assay buffer consisting of 20 mM HEPES (pH 7.4), 150 mM NaCl, 3% DMSO, and 0.05% Tween-20. The labeled protein was adjusted to a final concentration of 50 nM. Ligands were prepared as serial dilutions in identical assay buffer to ensure complete buffer matching across the titration series and to eliminate artifacts arising from differences in buffer composition or DMSO concentration. Binding reactions were assembled in 384-well assay plates compatible with the Dianthus NT.23 platform. Equal volumes of labeled protein and ligand solutions were combined to achieve the desired final concentrations. Samples were mixed gently and incubated for 30 minutes at room temperature protected from light to allow binding equilibrium to be established prior to measurement. Each titration series consisted of a broad concentration range designed to span concentrations below and above the expected affinity range of the interaction. Measurements were performed using instrument settings optimized during assay development to maximize signal-to-noise ratio while minimizing detector saturation and photobleaching. Initial fluorescence intensity was monitored for all wells prior to analysis to verify consistent fluorescence levels throughout the titration series. Wells exhibiting abnormal fluorescence intensities indicative of aggregation, precipitation, adsorption, quenching, or other assay artifacts were flagged during quality control evaluation. TRIC measurements were generated by applying a localized infrared laser-induced temperature jump to each sample and monitoring the resulting temperature-dependent fluorescence response of the labeled protein. Ligand binding alters the local environment, hydration shell, and molecular dynamics surrounding the fluorophore, resulting in measurable changes in fluorescence intensity following the temperature perturbation. The normalized TRIC signal was calculated automatically by the Dianthus NT Analysis software. Binding curves were generated by plotting the normalized TRIC response against ligand concentration and fitting the data using a one-site saturation binding model: $$\boldsymbol{Y = Bottom + \frac{(Top - Bottom) \times [L]}{K_{D,app} + [L]}}$$ where Y represents the normalized TRIC response, [L] is the ligand concentration, Top and Bottom correspond to the upper and lower asymptotes of the binding curve, and $K_{D,app}$ represents the apparent equilibrium dissociation constant under the assay conditions. All binding curves were visually inspected for assay quality prior to fitting. Quality control criteria included stable initial fluorescence across the titration series, absence of concentration-dependent fluorescence artifacts, reproducible signal amplitudes, consistent baselines, and the presence of a saturable binding response. In addition to affinity determination, TRIC traces were evaluated for evidence of non-specific interactions, colloidal aggregation, precipitation, adsorption effects, fluorescence quenching, or other concentration-dependent artifacts that could influence data interpretation. Apparent dissociation constants obtained by TRIC were compared with values obtained by differential scanning fluorimetry (DSF), fluorescence polarization (FP), and isothermal titration calorimetry (ITC) as part of an integrated orthogonal biophysical characterization strategy. Compounds demonstrating consistent binding behavior across multiple independent techniques were considered high-confidence binders. TRIC data were further used to support target engagement, rank compounds according to apparent affinity, and guide the selection of ligand concentrations used in subsequent structural and biophysical studies.
FP	Fluorescence polarization (FP) experiments were performed using a Tecan Infinite 1000 plate reader to evaluate binding of Target 1 to the fluorescent ligand analog provided by the client. The fluorescent probe consisted of the ligand labeled with Alexa Fluor 647. FP was used as a solution-phase binding assay to monitor changes in rotational diffusion of the fluorescent ligand upon binding to Target 1. All experiments were performed in assay buffer containing 20 mM HEPES (pH 7.4), 150 mM NaCl, 3% DMSO, and 0.05% Tween-20. Protein and fluorescent ligand solutions were prepared in identical buffer to maintain constant salt, detergent, and DMSO concentrations across the titration series. The Alexa Fluor 647–labeled ligand was diluted to a fixed final concentration, while Target 1 was prepared as a serial dilution to generate a protein-dependent binding curve. Reactions were assembled in a 384-well black, low-volume microplate suitable for fluorescence polarization measurements. Samples were mixed gently and incubated at room temperature protected from light to allow binding equilibrium to be established before measurement. Fluorescence polarization was measured using excitation and emission settings appropriate for Alexa Fluor 647. Parallel and perpendicular emission intensities were collected for each well using the plate reader polarization optics. Background fluorescence from buffer-only and protein-only wells was measured and subtracted when appropriate. Wells were evaluated for abnormal total fluorescence intensity to identify potential artifacts caused by fluorescence quenching, inner-filter effects, ligand aggregation, protein aggregation, precipitation, or compound interference.

The fluorescence polarization value was calculated from the parallel and perpendicular fluorescence intensities according to:

$$\boldsymbol{FP = \frac{I_{\parallel} - GI_{\perp}}{I_{\parallel} + GI_{\perp}}}$$

where $I_{\parallel}$is the fluorescence intensity detected parallel to the excitation plane, $I_{\perp}$is the fluorescence intensity detected perpendicular to the excitation plane, and $G$is the grating correction factor of the instrument.

Polarization values were reported in millipolarization units according to:

$$\boldsymbol{mP = 1000 \times FP}$$

When fluorescence anisotropy was calculated, anisotropy values were determined using:

$$\boldsymbol{r = \frac{I_{\parallel} - GI_{\perp}}{I_{\parallel} + 2GI_{\perp}}}$$

where $r$is fluorescence anisotropy. Binding was monitored as an increase or decrease in FP/mP signal resulting from the change in rotational mobility of the Alexa Fluor 647–labeled ligand upon association with Target 1. Binding curves were generated by plotting the corrected FP signal as a function of total Target 1 concentration. Data were fitted using a one-site binding model.

For conditions in which the concentration of fluorescent ligand was much lower than the expected KD, the binding response was fitted using the hyperbolic binding equation:

$$\boldsymbol{Y = Bottom + \frac{(Top - Bottom)[P]}{K_{D,app} + [P]}}$$

where $Y$is the observed FP signal, $Bottom$is the FP signal of free fluorescent ligand, $Top$is the FP signal at binding saturation, $[P]$is the total Target 1 concentration, and $K_{D,app}$is the apparent dissociation constant.

When the concentration of fluorescent ligand was not negligible relative to the expected KD, data were analyzed using the quadratic binding equation:

$$\boldsymbol{Y = Bottom + (Top - Bottom)\frac{([P]_T + [L]_T + K_D) - \sqrt{([P]_T + [L]_T + K_D)^2 - 4[P]_T[L]_T}}{2[L]_T}}$$

where $[P]_T$is the total protein concentration, $[L]_T$is the total fluorescent ligand concentration, $K_D$is the equilibrium dissociation constant, $Bottom$is the signal of free fluorescent ligand, and $Top$is the signal of the fully bound fluorescent ligand.

For competition experiments, unlabeled ligands were titrated against a pre-formed Target 1–Alexa Fluor 647 ligand complex. Displacement of the fluorescent ligand was monitored as a decrease in FP signal as a function of competitor concentration. Competition curves were fitted using a four-parameter logistic model:

$$\boldsymbol{Y = Bottom + \frac{Top - Bottom}{1 + 10^{(LogIC_{50} - X) \times HillSlope}}}$$

where $Y$is the FP signal, $X$is the logarithm of competitor concentration, $Top$and $Bottom$define the upper and lower plateaus, $LogIC_{50}$is the logarithm of the competitor concentration producing 50% displacement, and $HillSlope$describes the slope of the transition.

When appropriate, apparent inhibitor affinity was estimated from the measured IC50 using the Cheng–Prusoff relationship:

$$\boldsymbol{K_i = \frac{IC_{50}}{1 + \frac{[L]}{K_D}}}$$

where $K_i$is the apparent inhibition constant of the unlabeled ligand, $IC_{50}$is the half-maximal inhibitory concentration, $[L]$is the concentration of fluorescent ligand, and $K_D$is the dissociation constant of the fluorescent ligand–protein interaction determined from the direct-binding FP assay.

Raw parallel and perpendicular fluorescence intensities, total fluorescence intensity, calculated mP values, and fitted binding parameters were reviewed during data analysis. Data quality was assessed by evaluating signal window, replicate variability, total fluorescence stability, saturation behavior, and residuals from nonlinear regression fitting. Binding events were considered reliable when the FP response was concentration-dependent, saturable, reproducible across replicate wells, and not accompanied by large changes in total fluorescence

	intensity. Apparent affinity values obtained by FP were compared with TRIC, DSF, and ITC results as part of an orthogonal biophysical validation strategy.
ITC	Isothermal titration calorimetry (ITC) experiments were performed using a MicroCal ITC200 calorimeter (Malvern Panalytical) at 25°C. Prior to analysis, protein and ligand samples were prepared in matching buffers to minimize heats arising from buffer mismatch. The final ITC buffer consisted of 20 mM HEPES (pH 7.4), 150 mM NaCl, and 3% DMSO. Tween-20 was omitted from ITC experiments. DMSO concentrations were matched between the sample cell and syringe solutions. The sample cell (effective volume approximately 200 µL) was loaded with protein solution (25 µM), while the injection syringe (40 µL) was loaded with ligand solution (250 µM). Following an initial equilibration period of 600 s, titrations were performed using one preliminary injection of 0.4 µL, followed by 19 injections of 2.0 µL each with a spacing of 180 s between injections. The reference power was maintained at 8 µcal/s, and the stirring speed was set to 750 rpm throughout the experiment. Control titrations consisting of ligand into buffer and buffer into protein were performed when appropriate to evaluate heats of dilution. Raw thermograms were integrated using the manufacturer's software, and background heats were subtracted prior to fitting. Binding isotherms were analyzed using a single-site binding model to determine the equilibrium dissociation constant (K_D), binding stoichiometry (N), enthalpy change (ΔH), entropy contribution (−TΔS), and Gibbs free energy change (ΔG). Following completion of each titration, the contents of the ITC cell were recovered and used for orthogonal quality-control analyses including SDS-PAGE, circular dichroism (CD), analytical size-exclusion chromatography (aSEC), and differential scanning fluorimetry (DSF) to assess potential ligand-induced effects on protein integrity, secondary structure, oligomeric state, and aggregation behavior. **NOTE:** A water-to-water control and a $CaCl_2$–EDTA positive controls were performed periodically to verify instrument performance and baseline stability.
SPR	Binding interactions between Target 1 and the test ligands were characterized by surface plasmon resonance (SPR) using a Biacore instrument (Cytiva). All experiments were performed at 25 °C using HBS-based running buffer consisting of 20 mM HEPES (pH 7.4), 150 mM NaCl, 5% (v/v) DMSO, and 0.05% (v/v) Tween-20. Running buffer was freshly prepared, filtered (0.22 µm), and thoroughly degassed prior to use. Biotinylated Target 1 was immobilized onto a Series S Sensor Chip SA through the high-affinity biotin-streptavidin interaction. Immobilization levels were adjusted to approximately 300 response units (RU) on the active flow cell. A reference flow cell without immobilized protein was prepared in parallel and used for background subtraction. Ligands were prepared by serial dilution directly into running buffer, ensuring identical buffer composition and DMSO concentration between samples and running buffer to minimize bulk refractive index effects. Binding measurements were performed using a single-cycle kinetics (SCK) format in which increasing analyte concentrations were injected sequentially over the sensor surface without regeneration between injections. Following completion of the concentration series, a final dissociation phase was recorded to monitor complex stability. Sensorgrams were processed using Biacore Evaluation Software. Double referencing was applied by subtracting both the reference flow-cell response and blank buffer injections when appropriate. Experimental data were fitted globally to a 1:1 Langmuir binding model, yielding the association rate constant (k_{on}), dissociation rate constant (k_{off}), equilibrium dissociation constant (K_D), maximum binding response (R_{max}), and χ^2 goodness-of-fit values. Expected and observed *R*max values were compared to evaluate consistency with the assumed binding stoichiometry. Negative-control injections were performed using a reference ligand that does not interact with Target 1 under the experimental conditions, confirming that the observed responses originated from specific target engagement rather than nonspecific binding or bulk refractive index effects.

APPENDIX I

Raw data | Analyzed data | Location

SDS-PAGE

Target 1 APO	Target 1 +50 µM Ligand_1	Target 1 +50 µM Ligand_2
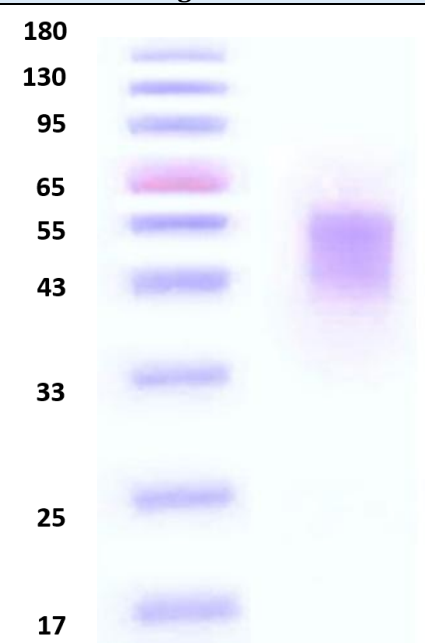	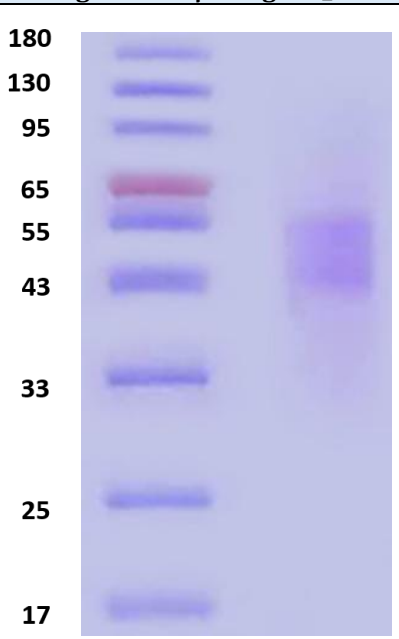	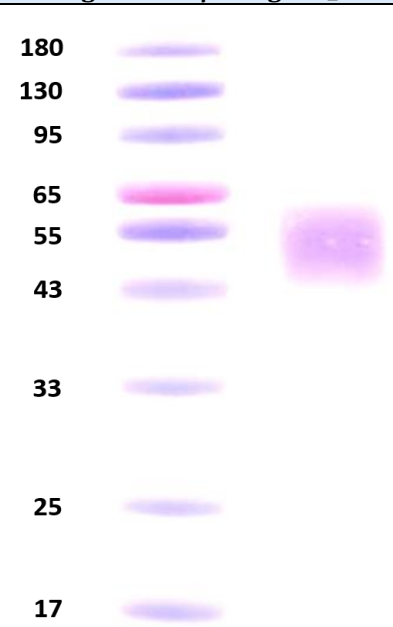
Raw data: **Analyzed data:**	**Raw data:** **Analyzed data:**	**Raw data:** **Analyzed data:**

Circular Dichroism

Target 1 APO	Target 1 + Ligand_1	Target 1 + Ligand_2
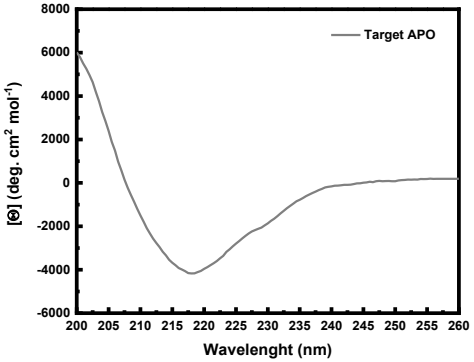	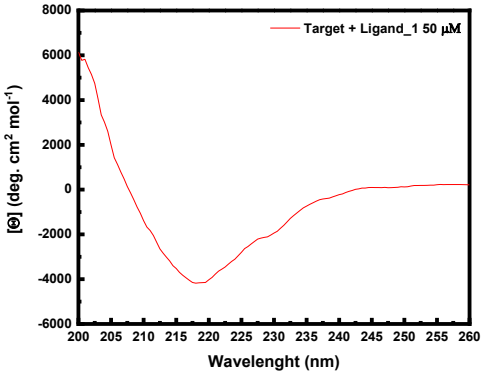	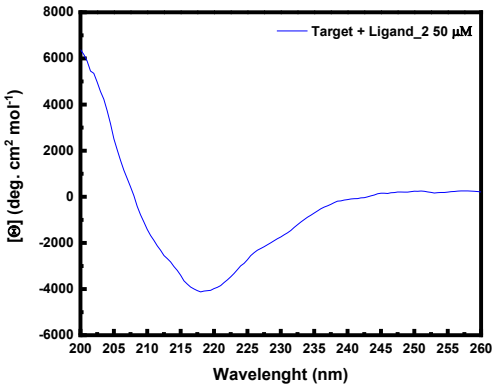
Raw data: **Analyzed data:**	**Raw data:** **Analyzed data:**	**Raw data:** **Analyzed data:**

aSEC

Target 1 APO	Target 1 + Ligand_1	Target 1 + Ligand_2
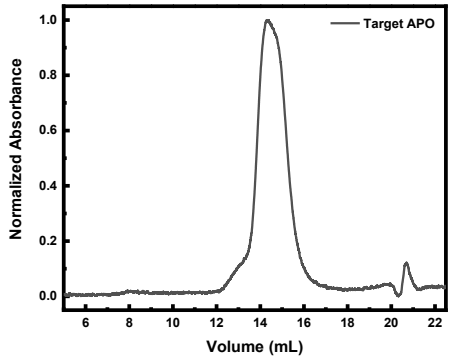	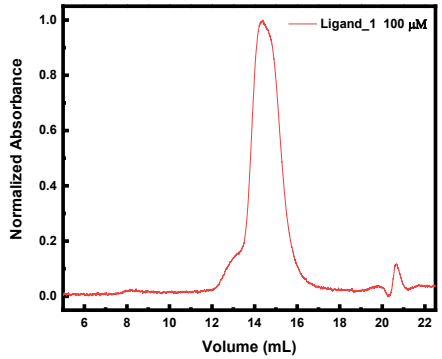	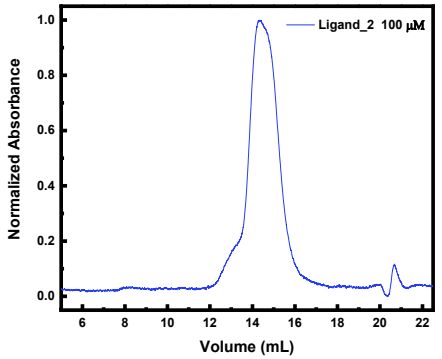
Raw data: **Analyzed data:**	**Raw data:** **Analyzed data:**	**Raw data:** **Analyzed data:**

DSF DMSO Effect

Target 1 DMSO stability

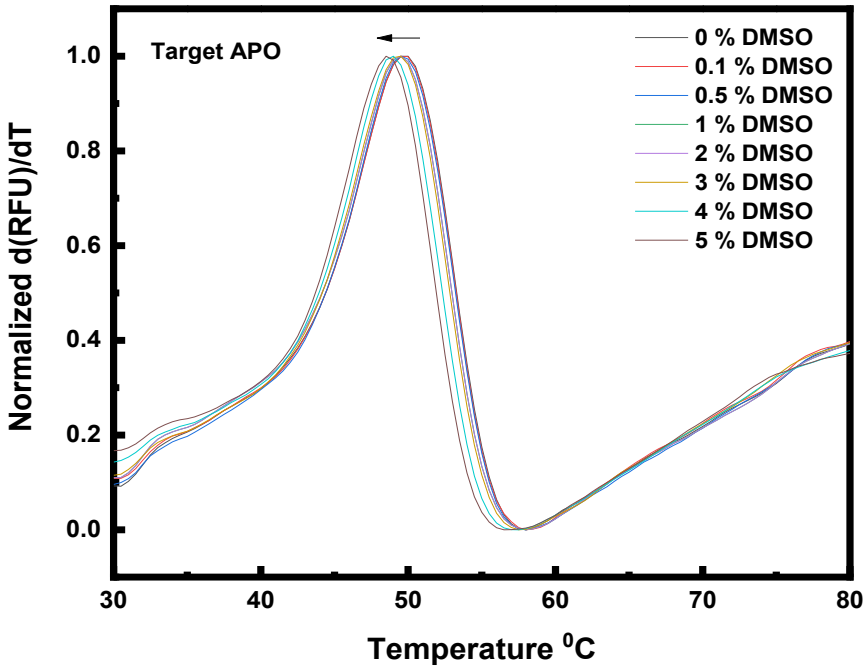

Raw data:
Analyzed data:

Sample	Raw data Plate Position	Raw data ID
Target 1 (apo)	A1;B1;C1	
Target 1 + 0.1 % DMSO	A2;B2;C2	
Target 1 + 0.5 % DMSO	A3;B3;C3	
Target 1 + 1 % DMSO	A4;B4;C4	
Target 1 + 2 % DMSO	A5;B5;C5	
Target 1 + 3 % DMSO	A6;B6;C6	
Target 1 + 4 % DMSO	A7;B7;C7	
Target 1 + 5 % DMSO	A8;B8;C8	

DSF $K_{D,app}$

Target 1 + Ligand_1 and Ligand_2
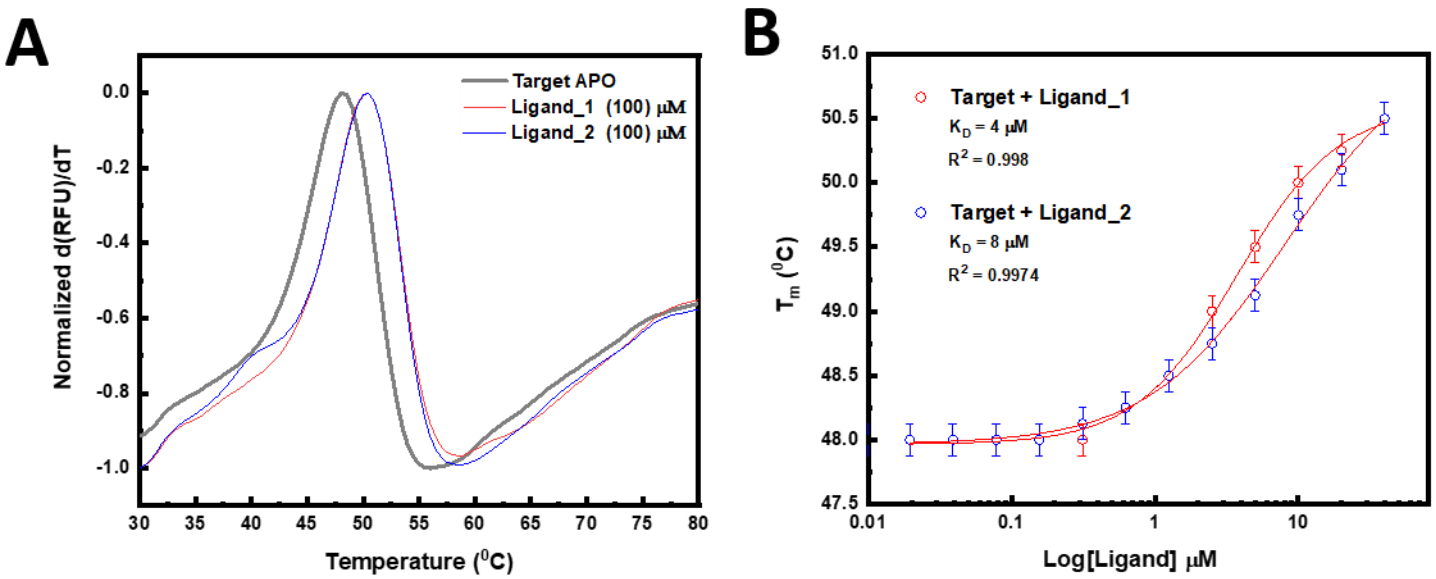
Raw data: **Analyzed data:**

Sample	**Raw data ID**
Target 1 (apo)	
Target 1 + Ligand_1_a (A)	
Target 1 + Ligand_1_b (B)	
Target 1 + Ligand_2_a (C)	
Target 1 + Ligand_2_b (D)	

Plate map

	Ligand concentration 40 µM to 20 nM at 2-fold dilution (µM)											
	1	**2**	**3**	**4**	**5**	**6**	**7**	**8**	**9**	**10**	**11**	**12**
A	40	20	10	5	2.5	1.25	0.6.25	0.315	0.16	0.08	0.04	0.02
B	40	20	10	5	2.5	1.25	0.6.25	0.315	0.16	0.08	0.04	0.02
C	40	20	10	5	2.5	1.25	0.6.25	0.315	0.16	0.08	0.04	0.02
D	40	20	10	5	2.5	1.25	0.6.25	0.315	0.16	0.08	0.04	0.02
E	0	0	0	0	0	0	0	0				
F												
G												
H												

E: Positive control (only Target 1)

TRIC $K_{D,app}$

Target 1 + Ligand_1 and Ligand_2

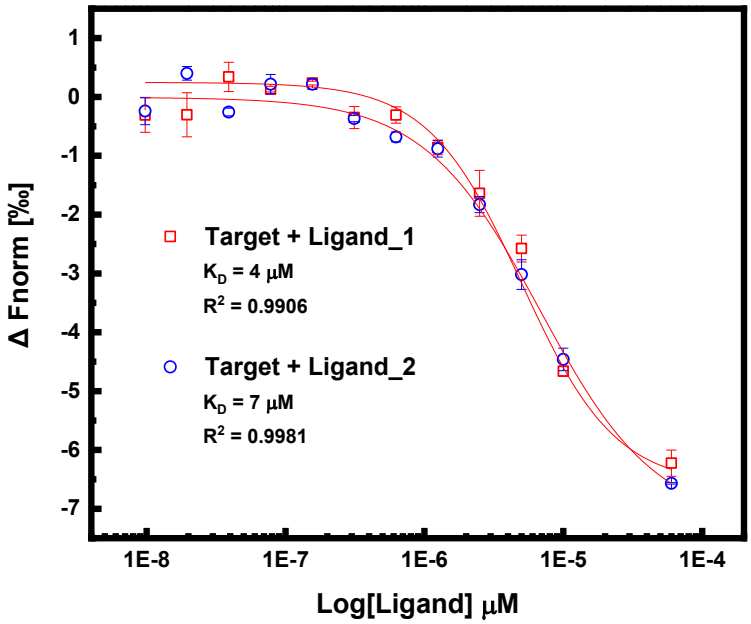

Raw data:
Analyzed data:

Sample	Raw data ID
Target 1 (apo)	
Target 1 + Ligand_1 (A-C)	
Target 1 + Ligand_2 (D-F)	

Plate map (384-well)

	Ligand concentration 60 µM to 5 nM at 2 fold dilution (µM)													
	1	**2**	**3**	**4**	**5**	**6**	**7**	**8**	**9**	**10**	**11**	**12**	**13**	**14**
A	60	20	10	5	2.5	1.25	0.6.25	0.315	0.16	0.08	0.04	0.02	0.01	0.005
B	60	20	10	5	2.5	1.25	0.6.25	0.315	0.16	0.08	0.04	0.02	0.01	0.005
C	60	20	10	5	2.5	1.25	0.6.25	0.315	0.16	0.08	0.04	0.02	0.01	0.005
D	60	20	10	5	2.5	1.25	0.6.25	0.315	0.16	0.08	0.04	0.02	0.01	0.005
E	60	20	10	5	2.5	1.25	0.6.25	0.315	0.16	0.08	0.04	0.02	0.01	0.005
F	60	20	10	5	2.5	1.25	0.6.25	0.315	0.16	0.08	0.04	0.02	0.01	0.005
G														
H														

A to C: Target 1 + Ligand_1; **D to F:** Target 1 + Ligand_2.

FP $K_{D,app}$

Target 1 + Ligand_1-Alexa643 and Ligand_2-Alexa643
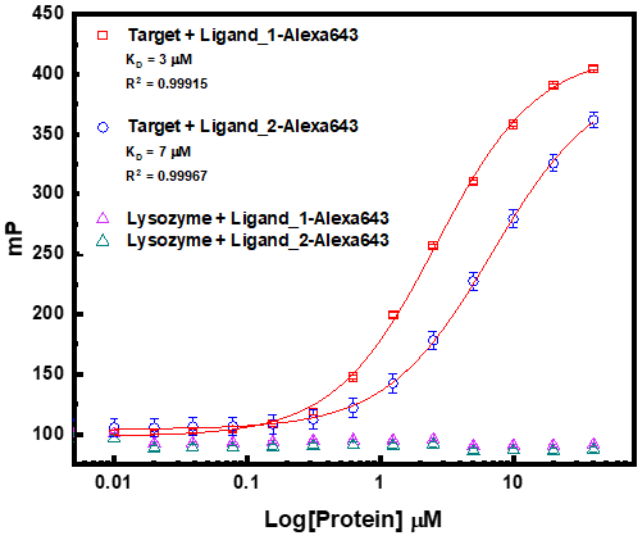 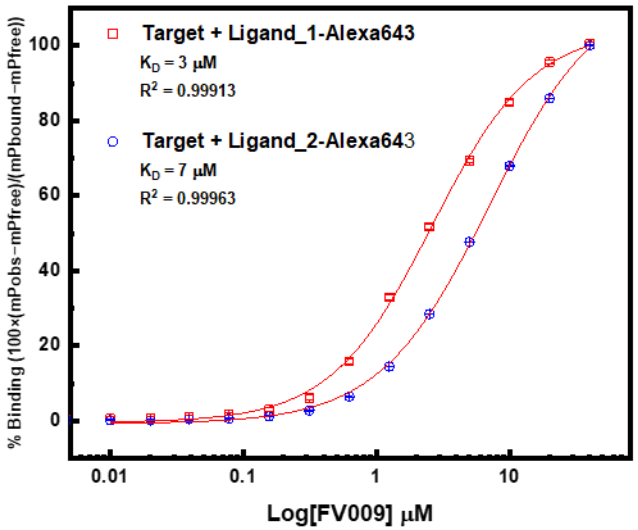
Raw data: **Analyzed data:**

Sample	Raw data ID
Target 1 (apo)	
Target 1 + Ligand_1-Alexa643 (A-C)	
Target 1 + Ligand_2-Alexa643 (D-F)	

Plate map (384-well)

	Protein concentration 40 µM to 10 nM at 2 fold dilution (µM)													
	1	**2**	**3**	**4**	**5**	**6**	**7**	**8**	**9**	**10**	**11**	**12**	**13**	**14**
A	40	20	10	5	2.5	1.25	0.6.25	0.315	0.16	0.08	0.04	0.02	0.01	0
B	40	20	10	5	2.5	1.25	0.6.25	0.315	0.16	0.08	0.04	0.02	0.01	0
C	40	20	10	5	2.5	1.25	0.6.25	0.315	0.16	0.08	0.04	0.02	0.01	0
D	40	20	10	5	2.5	1.25	0.6.25	0.315	0.16	0.08	0.04	0.02	0.01	0
E	60	20	10	5	2.5	1.25	0.6.25	0.315	0.16	0.08	0.04	0.02	0.01	0
F	40	20	10	5	2.5	1.25	0.6.25	0.315	0.16	0.08	0.04	0.02	0.01	0
G	40	20	10	5	2.5	1.25	0.6.25	0.315	0.16	0.08	0.04	0.02	0.01	0
H	40	20	10	5	2.5	1.25	0.6.25	0.315	0.16	0.08	0.04	0.02	0.01	0
I	40	20	10	5	2.5	1.25	0.6.25	0.315	0.16	0.08	0.04	0.02	0.01	0
J	40	20	10	5	2.5	1.25	0.6.25	0.315	0.16	0.08	0.04	0.02	0.01	0
K	40	20	10	5	2.5	1.25	0.6.25	0.315	0.16	0.08	0.04	0.02	0.01	0
L	40	20	10	5	2.5	1.25	0.6.25	0.315	0.16	0.08	0.04	0.02	0.01	0
M	40	20	10	5	2.5	1.25	0.6.25	0.315	0.16	0.08	0.04	0.02	0.01	0

A to C: 10 nM Ligand_1-Alexa643 + Target 1 dose response; **D to F:** 10 nM Ligand_2-Alexa643 + Target 1 dose response; **G to H:** 10 nM Ligand_1-Alexa643 + Lysozyme dose response and **I to J:** 10 nM Ligand_2-Alexa643 + Lysozyme dose response

ITC Data

1. QUALITY CONTROL

Water-water	Buffer-Buffer	$CaCl_2$-EDTA
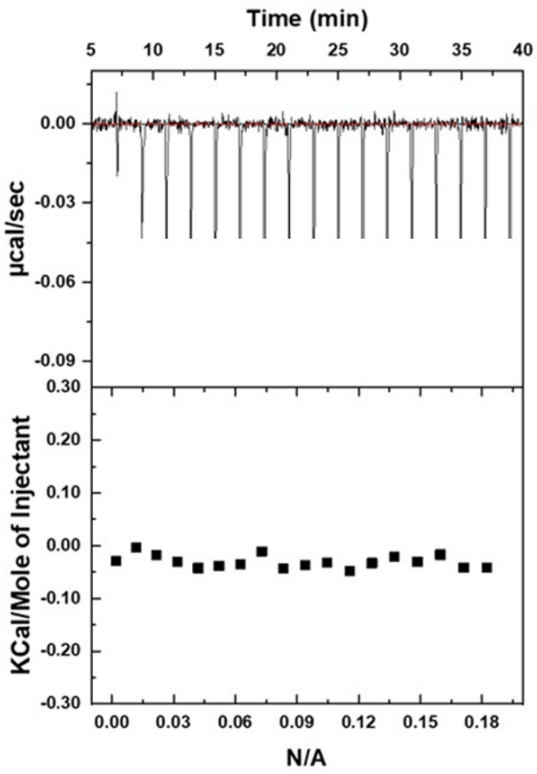	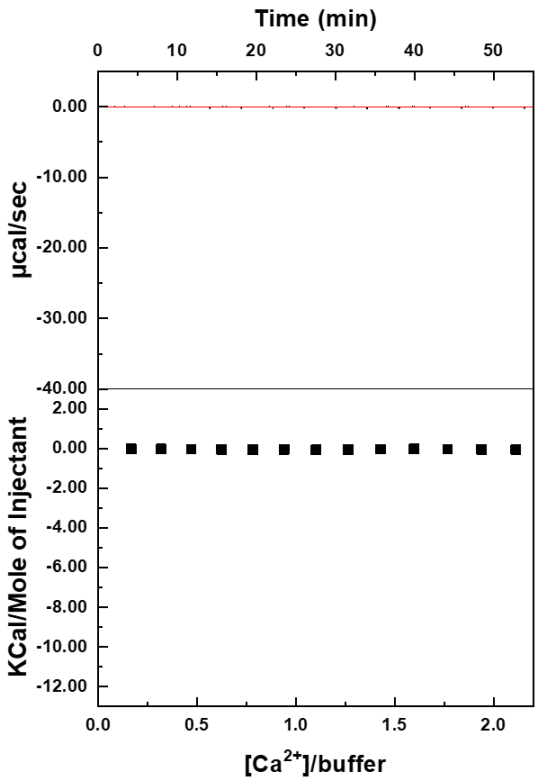	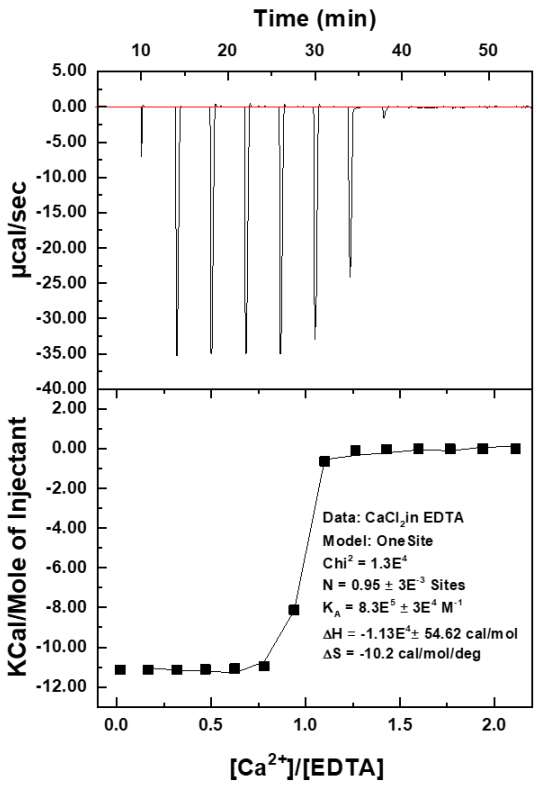
Raw data: **Analyzed data:**	**Raw data:** **Analyzed data:**	**Raw data:** **Analyzed data:**

Buffer: 20 mM Hepes (pH=7.4), 150 mM NaCl, 5% DMSO

2. ITC LIGANDS LIGAND_1 AND LIGAND_2 IN BUFFER

Ligand_1-Buffer	Ligand_2-Buffer
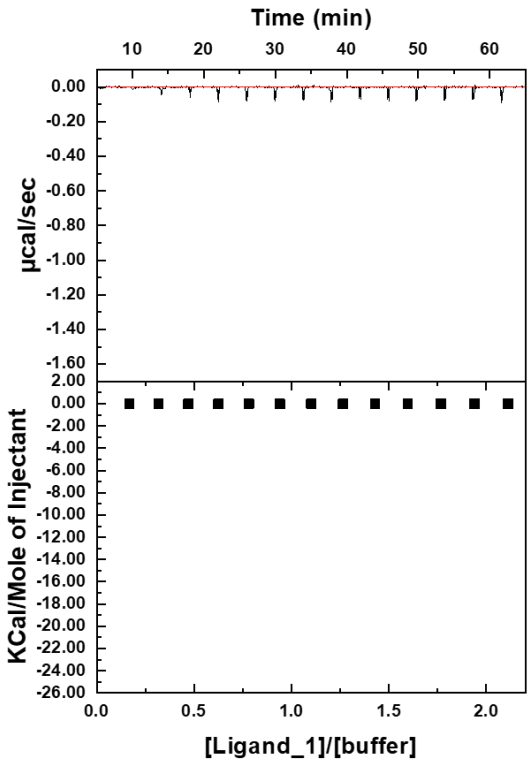	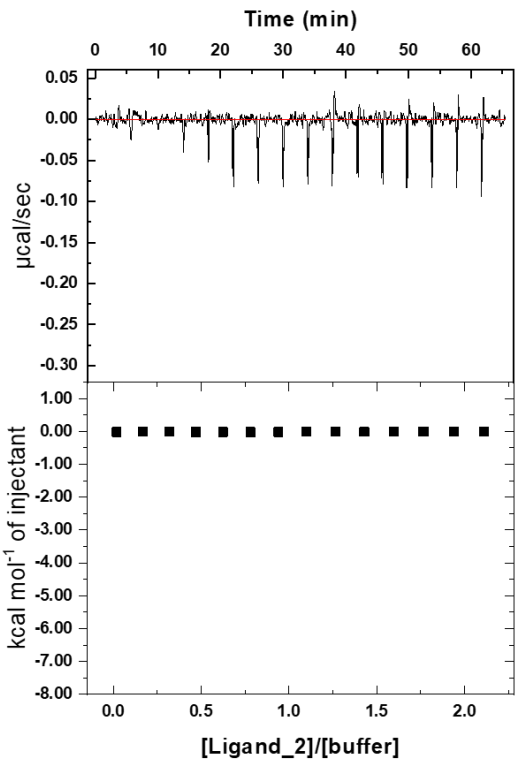
Raw data: **Analyzed data:**	**Raw data:** **Analyzed data:**

Buffer: 20 mM Hepes (pH=7.4), 150 mM NaCl, 5% DMSO

3. ITC LIGANDS LIGAND_1 AND LIGAND_2

Ligand_1-Target	Ligand_2-Target
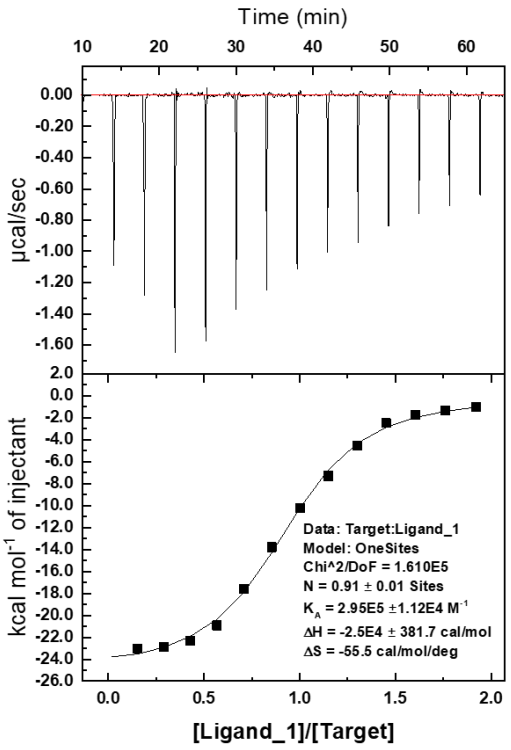	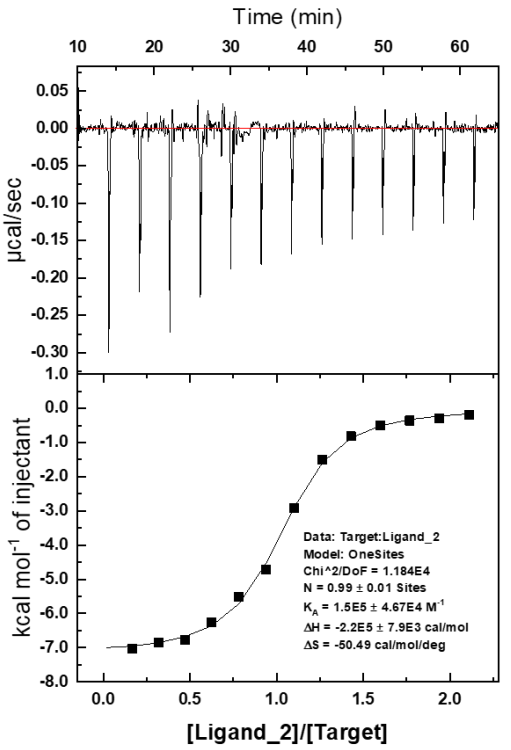
Raw data: **Analyzed data:**	**Raw data:** **Analyzed data:**

Buffer: 20 mM Hepes (pH=7.4), 150 mM NaCl, 5% DMSO

SPR Binding and kinetics

1. TARGET:LIGAND_1, TARGET:LIGAND_2 AND TARGET:BUFFER

Ligand_1 flow on Target	Ligand_2 flow on Target	buffer flow on Target
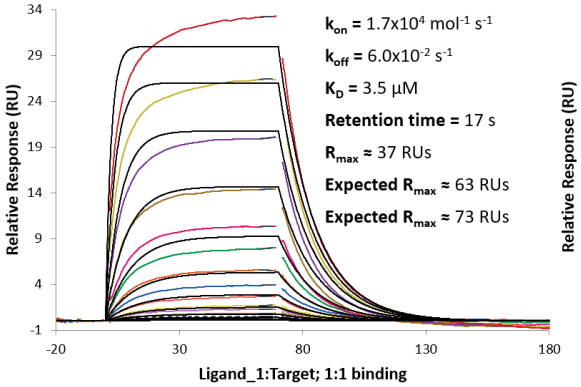	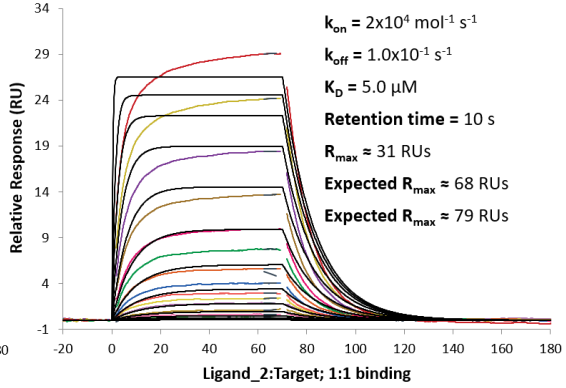	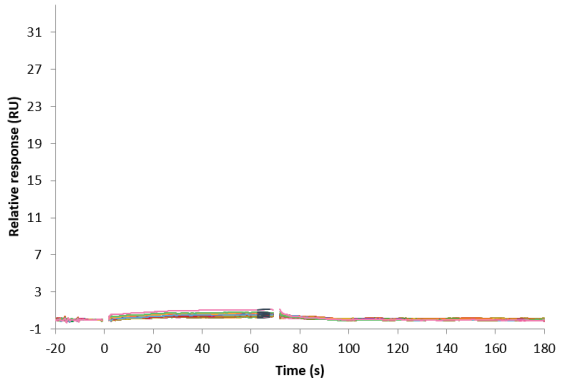
Raw data: **Analyzed data:**	**Raw data:** **Analyzed data:**	**Raw data:** **Analyzed data:**

Buffer: 20 mM Hepes (pH=7.4), 150 mM NaCl, 5% DMSO + 0.05% Tween

2. STEADY-STATE AFFINITY AND OCCUPANCY

Target 1 + Ligand_1 and Ligand_2 RU versus [Ligand]

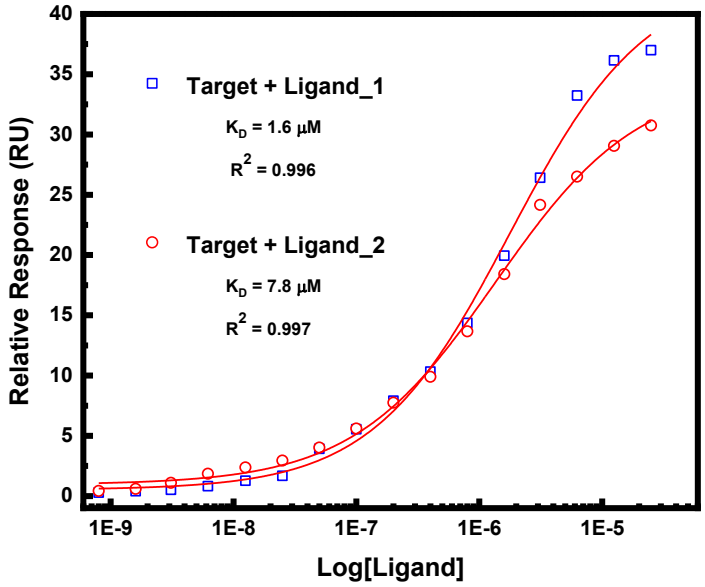

Raw data:
Analyzed data: